Mon. Not. R. Astron. Soc. **419,** 2587–2605 (2012) doi:10.1111/j.1365-2966.2011.19908.x

Broad-band optical polarimetric studies towards the Galactic young star cluster Berkeley 59

C. Eswaraiah,[1★] A. K. Pandey,[1] G. Maheswar,[1] W. P. Chen,[2] D. K. Ojha[3] and H. C. Chandola[4]

[1]*Aryabhatta Research Institute of Observational Sciences, Manora Peak, Nainital 263129, India*
[2]*Institute of Astronomy, National Central University, Chung-Li 32054, Taiwan*
[3]*Tata Institute of Fundamental Research, Mumbai 400005, India*
[4]*Department of Physics, Kumaun University, Nainital 263129, India*

Accepted 2011 September 27. Received 2011 September 27; in original form 2011 September 1

ABSTRACT

We present multiwavelength optical linear polarimetric observations of 69 stars towards the young open cluster Berkeley 59. The observations reveal the presence of three dust layers located at distances of ∼300, ∼500 and ∼700 pc. The dust layers produce a total polarization $P_V \sim 5.5$ per cent. The mean values of polarization and polarization angles due to the dust layers are found to increase systematically with distance. We show that polarimetry in combination with the $(U - B)$–$(B - V)$ colour–colour diagram yields a better identification of cluster members. The polarization measurements suggest that the polarization due the intracluster medium is ∼2.2 per cent. An anomalous reddening law exists for the cluster region, indicating a relatively larger grain size than that in the diffuse interstellar medium. The spatial variation of polarization and colour excess $E(B - V)$ are found to increase with radial distance from the cluster centre, whereas θ_V and λ_{max} are found to decrease with increasing radial distance from the cluster centre. About 40 per cent of cluster members show the signatures of either intrinsic polarization or rotation in their polarization angles. There is an indication that the starlight of the cluster members might have been depolarized because of non-uniform alignment of dust grains in the foreground dust layers and in the intracluster medium.

Key words: polarization – dust, extinction – open clusters and associations: individual: Berkeley 59.

1 INTRODUCTION

Interstellar grains are aspherical in nature and, given proper conditions, are aligned in space by the magnetic field (cf. Davis & Greenstein 1951; Lazarian 2007; Lazarian & Hoang 2007; Andersson et al. 2011). The effective extinction cross-sections of the dust particles are the greatest when the electric vector of the incident light is parallel to the long axes of the dust particles as projected on the plane of the sky, and the least when parallel to the short axes. This differential extinction introduces a small degree of linear polarization in the transmitted light.

Studies of polarization due to the interstellar medium (ISM) are important as these provide information about the properties of the dust associated with the ISM and intracluster medium as well as help to trace the Galactic magnetic field. As the grains are thought to align due to the local magnetic field, the observed polarization vectors map the general geometry of the magnetic field. The observed maximum upper limit relation between the degree of polarization and the colour excess $E(B - V)$ is found to be $P_{max} = 9 \times E(B - V)$ (Aannestad & Purcell 1973). The relation between P_{max} and colour excess, and the variation in P with wavelength are interpreted in terms of the grain properties and the efficiency of the grain alignment. Therefore, polarimetry is a useful technique to investigate the properties like maximum polarization $P_{\lambda_{max}}$, the wavelength λ_{max} corresponding to $P_{\lambda_{max}}$, and the orientation of the magnetic field in various Galactic locations.

Polarimetric studies of star-forming regions/young star clusters are specially important because physical parameters such as distance, age, membership and colour excess $E(B - V)$ of these regions are known accurately, which consequently helps in analysing the polarimetric data in a meaningful way. Strong ultraviolet radiation from O/B-type stars in these regions has strong impact on the surrounding medium. Dust grains can undergo destruction processes due to direct radiative pressure, grain–grain collisions, sputtering or shattering, etc. As a result, it is likely that the mean size of the dust grains could be smaller than the mean value for the diffuse ISM. The stars associated with the star-forming regions can help to

★E-mail: eswar@aries.res.in

understand the nature of dust as well as the magnetic field of the intracluster medium.

Young star clusters (age < 10 Myr), still embedded in the parent molecular clouds, are unique laboratories to understand the dust properties as well as the nature of interaction between young star(s) and the surrounding medium. Berkeley 59 (Be 59; $\alpha_{2000} = 00^{h}02^{m}13^{s}, \delta_{2000} = +67^{\circ}25'11''$; $l = 118\overset{\circ}{.}22$, $b = 5\overset{\circ}{.}00$) is such a young star cluster associated with a heavily obscured gas–dust complex of the Cepheus OB4 association. The cluster Be 59, located at the centre of the Sharpless 171 region, contains nine O7–B3 stars (cf. Pandey et al. 2008, hereinafter P08) at a distance of 1.00 ± 0.05 kpc and has $E(B - V) \simeq 1.4$ to 1.8 mag. The extent of the cluster was found to be 2.9 pc (P08).

As a part of an ongoing project to understand the dust characteristics in star-forming regions and to map the structure of magnetic field at diverse environments of the Milky Way, we have carried out broad-band optical polarimetric observations around the cluster Be 59. In Section 2, we present the observations and data reduction. Results are presented in Section 3. The dust properties and the spatial variation of $E(B - V)$, P_V, θ_V and λ_{max} are discussed in Sections 4 and 5, respectively. Finally, we report our conclusions in Section 6.

2 OBSERVATIONS AND DATA REDUCTION

Polarimetric observations were carried out on seven nights (2009 November 23, 24, 25 and 2009 December 24, 26, 27 and 28), using the ARIES Imaging Polarimeter (AIMPOL; Rautela, Joshi & Pandey 2004) mounted at the Cassegrain focus of the 104-cm Sampurnanand telescope of the Aryabhatta Research Institute of Observational Sciences (ARIES), Nainital, India. The observations were carried out in the $BV(RI)_C$ photometric bands ($\lambda_{B_{eff}} = 0.440\,\mu$m, $\lambda_{V_{eff}} = 0.530\,\mu$m, $\lambda_{R_{eff}} = 0.670\,\mu$m and $\lambda_{I_{eff}} = 0.800\,\mu$m) using a fraction (370 × 370 pixel^2) of the TK 1024 × 1024 pixel^2 CCD camera. The AIMPOL consists of a half-wave plate modulator and a Wollaston prism beam-splitter. The Wollaston prism analyser is placed at the backend of the telescope beam path in order to produce ordinary and extraordinary beams in slightly different directions separated by 28 pixels along the north–south direction on the sky plane. A focal reducer (85 mm, f/1.8) is placed between the Wollaston prism and the CCD camera. Each pixel of the CCD corresponds to 1.73 arcsec and the field of view is ~8 arcmin diameter on the sky. The full width at half-maximum of the stellar image varied from 2 to 3 pixels. The readout noise and gain of the CCD are 7.0 e^{-1} and 11.98 e^{-1} ADU^{-1}, respectively. Since the AIMPOL does not have a grid, we manually checked for any overlap of ordinary and extraordinary images of the sources. Fluxes of ordinary (I_o) and extraordinary (I_e) beams for all the observed sources with good signal-to-noise ratio were extracted by standard aperture photometry after bias subtraction using the IRAF[1] package. The ratio $R(\alpha)$ is computed using the following relation:

$$R(\alpha) = \frac{[I_e(\alpha)/I_o(\alpha)] - 1}{[I_e(\alpha)/I_o(\alpha)] + 1} = P\cos(2\theta - 4\alpha), \quad (1)$$

where P is the fraction of the total light in the linearly polarized condition and θ is the position angle of the plane of polarization. Here α is the position of the fast axis of the half-wave plate at 0°, $22\overset{\circ}{.}5$, 45° and $67\overset{\circ}{.}5$ corresponding to the four normalized Stokes parameters, respectively, q [$R(0°)$], u [$R(22\overset{\circ}{.}5)$], q_1 [$R(45°)$] and u_1 [$R(67\overset{\circ}{.}5)$]. The detailed procedures used to estimate the polarization and position angles for the programme stars are given by Eswaraiah et al. (2011, hereinafter E11), and references therein.

The instrumental polarization of the AIMPOL on the 104-cm Sampurnanand telescope has been monitored since 2004 on various observing nights and found to be less than 0.1 per cent in different bands (E11, and references therein). All the measurements were corrected for both the null polarization (~0.1 per cent), which is independent of the passbands, and the zero-point polarization angle by observing several unpolarized and polarized standard stars from Schmidt, Elston & Lupie (1992, hereinafter S92). The results for the standard stars are given in Table 1. The first column lists the star name with the date of observation or reference in parentheses. The next consecutive columns are the polarization in per cent [P (per cent)] and polarization angle in degrees [$\theta(°)$] measured in the $BV(RI)_C$ passbands. The entries with S92 in parentheses are taken from S92. The present results for the polarized standard stars are in good agreement, within the observational errors, with those given by S92.

3 RESULTS

Table 2 lists the polarization measurements for 37 stars using the $BV(RI)_C$ bands, whereas Table 3 lists the results for 32 stars using the $V(RI)_C$ bands. The star identification numbers (column 1) are taken from P08. The right ascension, declination and photometric visual magnitudes, also from P08, are listed in the second, third and fourth columns, respectively, of Tables 2 and 3. The next consecutive columns of Tables 2 and 3 correspond to the polarization, polarization angle and their associated errors in the $BV(RI)_C$ and $V(RI)_C$ passbands, respectively. The given polarization angles are in the equatorial coordinate system measured from the north increasing towards the east. Tables 2 and 3 reveal that the maximum linear polarization towards the cluster region is ~8 per cent. Such a high amount of polarization is not often found towards star clusters, with only a few exceptions, for example, Trumpler 27 (Feinstein et al. 2000) and M17 (Schulz et al. 1981).

In Fig. 1, all the observed 69 stars are marked with the white circles on the DSS II R-band image. The sky projection of V-band polarization vectors is overlaid. The length of each polarization vector is proportional to the degree of polarization. The dot–dashed line represents the orientation of the projection of the Galactic plane (GP) at $b = 5\overset{\circ}{.}03$, which corresponds to a position angle of 86°.

3.1 Distribution of P_V and θ_V

A careful inspection of Fig. 1 reveals two groups of stars characterized by different degrees and directions of polarization. The first group with relatively small degree of polarization (~2 per cent) and with the orientation nearly parallel to the Galactic disc (~86°) may be composed of foreground stars. The stars of this group are randomly distributed on the plane of the sky. The second group, whose degree of polarization is significantly higher than the first group and the alignment of polarization vectors (~102°) is significantly deviated from the GP, may be composed of cluster members. The majority of the stars in the second group are located within the cluster region (~10 arcmin).

Fig. 2 displays the distribution of polarization P_V versus polarization angle θ_V, which clearly segregates the above-mentioned two groups. The mean P_V and θ_V for the first group are found to be

[1] IRAF is distributed by the National Optical Astronomical Observatories, USA.

Table 1. Observed polarized standard stars from S92.

Star name (date of observation) (reference) (1)	$P_B \pm \epsilon$ (per cent) (2)	$\theta_B \pm \epsilon$ (°) (3)	$P_V \pm \epsilon$ (per cent) (4)	$\theta_V \pm \epsilon$ (°) (5)	$P_{R_C} \pm \epsilon$ (per cent) (6)	$\theta_{R_C} \pm \epsilon$ (°) (7)	$P_{I_C} \pm \epsilon$ (per cent) (8)	$\theta_{I_C} \pm \epsilon$ (°) (9)
HD 19820 (2009 November 23)	4.49 ± 0.11	114.9 ± 0.7	4.89 ± 0.09	114.2 ± 0.5	4.49 ± 0.09	115.5 ± 0.6	4.06 ± 0.16	115.3 ± 1.0
HD 19820 (2009 November 24)	4.61 ± 0.11	114.7 ± 0.7	4.79 ± 0.08	115.1 ± 0.5	4.51 ± 0.07	114.6 ± 0.4	3.97 ± 0.09	115.7 ± 0.6
HD 19820 (2009 November 25)	4.72 ± 0.11	115.6 ± 0.7	4.94 ± 0.08	114.9 ± 0.4	4.61 ± 0.07	114.4 ± 0.4	3.86 ± 0.10	113.4 ± 0.7
HD 19820 (2009 December 23)	4.70 ± 0.10	115.0 ± 0.6	–	–	4.61 ± 0.07	114.3 ± 0.4	4.06 ± 0.08	114.0 ± 0.5
HD 19820 (2009 December 24)	4.68 ± 0.11	116.4 ± 0.7	4.90 ± 0.09	114.6 ± 0.5	4.62 ± 0.07	114.8 ± 0.4	4.06 ± 0.08	114.3 ± 0.5
HD 19820 (2009 December 27)	4.57 ± 0.11	116.4 ± 0.6	4.69 ± 0.09	115.0 ± 0.5	4.63 ± 0.07	114.6 ± 0.4	4.01 ± 0.08	114.3 ± 0.5
HD 19820 (2009 December 28)	4.72 ± 0.09	115.4 ± 0.5	4.80 ± 0.08	114.8 ± 0.5	4.51 ± 0.07	114.2 ± 0.4	3.92 ± 0.08	115.2 ± 0.5
HD 19820 (S92)	4.70 ± 0.04	115.7 ± 0.2	4.79 ± 0.03	114.9 ± 0.2	4.53 ± 0.03	114.5 ± 0.2	4.08 ±0.02	114.5 ± 0.2
HD 25443 (2009 November 23)	5.19 ± 0.09	134.6 ± 0.5	5.04 ± 0.07	136.0 ± 0.4	5.01 ± 0.06	134.5 ± 0.4	4.19 ± 0.09	134.8 ± 0.6
HD 25443 (2009 November 24)	5.21 ± 0.09	134.1 ± 0.5	5.11 ± 0.07	136.2 ± 0.4	5.13 ± 0.06	133.8 ± 0.4	4.29 ± 0.09	134.4 ± 0.6
HD 25443 (2009 November 25)	5.11 ± 0.09	134.5 ± 0.5	5.25 ± 0.09	134.3 ± 0.5	5.10 ± 0.08	133.4 ± 0.4	4.37 ± 0.10	132.6 ± 0.7
HD 25443 (2009 December 23)	5.12 ± 0.08	135.7 ± 0.5	5.12 ± 0.08	135.5 ± 0.4	4.88 ± 0.08	134.5 ± 0.5	4.23 ± 0.08	134.9 ± 0.5
HD 25443 (2009 December 24)	5.12 ± 0.09	134.0 ± 0.5	5.27 ± 0.09	134.8 ± 0.5	5.00 ± 0.08	134.5 ± 0.4	4.19 ± 0.07	136.0 ± 0.5
HD 25443 (2009 December 27)	5.05 ± 0.08	134.8 ± 0.5	5.17 ± 0.07	135.9 ± 0.4	5.04 ± 0.07	134.0 ± 0.4	4.13 ± 0.07	134.5 ± 0.5
HD 25443 (S92)	5.23 ± 0.09	134.3 ± 0.5	5.13 ± 0.06	134.2 ± 0.3	4.73 ± 0.05	133.6 ± 0.3	4.25 ± 0.04	134.2 ± 0.3
BD + 64° 106 (2009 November 23)	5.49 ± 0.17	98.0 ± 0.9	6.09 ± 0.13	99.0 ± 0.6	5.41 ± 0.11	96.1 ± 0.6	4.50 ± 0.14	96.6 ± 0.9
BD + 64° 106 (2009 December 23)	5.37 ± 0.15	97.9 ± 0.8	5.57 ± 0.11	96.8 ± 0.6	5.63 ± 0.09	97.6 ± 0.5	4.63 ± 0.10	97.5 ± 0.6
BD + 64° 106 (S92)	5.51 ± 0.09	97.2 ± 0.5	5.69 ± 0.04	96.6 ± 0.2	5.15 ± 0.10	96.7 ± 0.5	4.70 ± 0.05	96.9 ± 0.3
HD 204827 (2009 November 25)	5.67 ± 0.10	58.3 ± 0.5	5.53 ± 0.08	58.8 ± 0.4	5.02 ± 0.08	59.2 ± 0.4	4.14 ± 0.10	59.9 ± 0.7
HD 204827 (S92)	5.65 ± 0.02	58.2 ± 0.1	5.32 ± 0.01	58.7 ± 0.1	4.89 ± 0.03	59.1 ± 0.2	4.19 ± 0.03	59.9 ± 0.2
BD + 59° 389 (2009 December 23)	6.35 ± 0.13	97.8 ± 0.6	6.73 ± 0.09	97.8 ± 0.4	6.48 ± 0.08	97.6 ± 0.3	5.66 ± 0.06	97.9 ± 0.3
BD + 59° 389 (2009 December 28)	6.43 ± 0.13	97.9 ± 0.6	6.82 ± 0.09	97.5 ± 0.4	6.47 ± 0.08	97.7 ± 0.4	5.61 ± 0.07	97.9 ± 0.4
BD + 59° 389 (S92)	6.34 ± 0.04	98.1 ± 0.2	6.70 ± 0.01	98.1 ± 0.1	6.43 ± 0.02	98.1 ± 0.1	5.80 ± 0.02	98.3 ± 0.1
HD 236633 (2009 December 28)	6.06 ± 0.11	90.4 ± 0.5	5.65 ± 0.09	91.3 ± 0.4	5.34 ± 0.09	91.0 ± 0.5	4.69 ± 0.09	90.5 ± 0.6
HD 236633 (S92)	5.53 ± 0.04	92.5 ± 0.2	5.49 ± 0.02	93.8 ± 0.1	5.38 ± 0.03	93.0 ± 0.2	4.80 ± 0.04	93.1 ± 0.2

2.47 ± 0.46 per cent and $81° \pm 9°$, respectively. The mean polarization angle is nearly aligned with the GP, indicating homogeneity in the *local magnetic field* of the Galaxy towards the direction of Be 59. The stars belonging to the second group are more polarized ($P_V \gtrsim 4.0$ per cent) and having $\theta_V \gtrsim 90°$. The mean polarization angle of the second group ($103° \pm 5°$) significantly deviates from the GP. The magnetic field associated with the parental molecular cloud may have been perturbed during the cloud collapse or due to the strong stellar winds or supernova explosions (e.g. Waldhausen, Martínez & Feinstein 1999). The stars belonging to the second group could be either the cluster members or background stars. The second group of stars show large dispersion in polarization but a very small dispersion in polarization angle. The large dispersion in P_V (4–8.7 per cent) could be attributed to the differential reddening within the cluster. A similar type of segregated groups have already been reported in a few cases, namely Trumpler 27 (Feinstein et al. 2000), Hogg 22 and NGC 6204 (Martínez, Vergne & Feinstein 2004), NGC 5749 (Vergne, Feinstein & Martínez 2007) and NGC 6250 (Feinstein et al. 2008).

The distribution of P_V for all the observed 69 stars is shown in the upper panel of Fig. 3, which clearly reveals two separate distributions for field and probable cluster members. The distribution for field stars peaks at ∼2 per cent, whereas that for the probable members peaks at 5.5 per cent with an extended tail towards higher polarization, which could be either due to highly extincted probable members, background stars or due to the presence of different populations of dust grains with different polarizing properties. The lower panel of Fig. 3 shows the distribution of θ_V, which reveals that the distribution of probable cluster members lies in the range of 95°–115° with a peak at ∼105°.

To have a better understanding of the nature of the dust component and the magnetic field associated with the foreground and intracluster medium, it is essential to find out the members associated with the cluster versus the stars located in the foreground/background of the cluster. In our previous study (E11), we have shown that polarimetry in combination with the $(U - B)$–$(B - V)$ two-colour diagram (TCD) can yield a better identification of probable members than photometry alone. In the ensuing section, we will discuss the determination of membership using the polarization properties in combination with the $(U - B)$–$(B - V)$ TCD.

3.2 Member identification

The $(U - B)$–$(B - V)$ TCD is one of the useful tools to identify probable members of a cluster. It is expected that all member stars have $E(B - V)$ values comparable to the mean $E(B - V)$ value of the cluster since the cluster stars have formed out of the same molecular cloud and consequently have the same distance and age. In comparison, the field population are expected to be less or highly extincted depending on whether they are foreground or background to the cluster. Fig. 4 shows the $(U - B)$–$(B - V)$ TCD for only 63 stars as the $U - B$ colour is not available for six stars. In Fig. 4, the zero-age main sequence (ZAMS) from Schmidt-Kaler (1982) is shifted along a normal reddening vector having a slope of $E(U - B)/E(B - V) = 0.72$. The TCD shows a variable reddening in the cluster region with $E(B - V)_{\rm min} \sim 1.4$ mag and

Table 2. Observed $BV(RI)_C$ polarization and polarization angles for 37 stars towards Be 59.

Star ID[a] (1)	RA (°) (J2000) (2)	Dec. (°) (J2000) (3)	V (mag)[a] (4)	$P_B \pm \epsilon$ (per cent) (5)	$\theta_B \pm \epsilon$ (°) (6)	$P_V \pm \epsilon$ (per cent) (7)	$\theta_V \pm \epsilon$ (°) (8)	$P_{R_C} \pm \epsilon$ (per cent) (9)	$\theta_{R_C} \pm \epsilon$ (°) (10)	$P_{I_C} \pm \epsilon$ (per cent) (11)	$\theta_{I_C} \pm \epsilon$ (°) (12)
3	0.55659104	67.417798	11.30	4.80 ± 0.20	102.3 ± 1.2	5.30 ± 0.13	105.1 ± 0.7	5.00 ± 0.10	104.0 ± 0.5	4.57 ± 0.09	106.7 ± 0.6
15	0.50060639	67.419664	12.78	5.04 ± 0.41	103.4 ± 2.3	5.85 ± 0.26	103.6 ± 1.2	6.20 ± 0.19	103.4 ± 0.9	5.48 ± 0.18	104.4 ± 0.9
16	0.57895372	67.427389	11.81	6.87 ± 0.31	106.8 ± 1.3	7.55 ± 0.16	104.9 ± 0.6	7.04 ± 0.09	106.0 ± 0.4	6.68 ± 0.07	107.7 ± 0.3
16A	0.54241389	67.429288	–	5.35 ± 0.09	106.3 ± 0.5	5.53 ± 0.06	107.7 ± 0.3	5.45 ± 0.04	106.4 ± 0.2	4.64 ± 0.04	106.5 ± 0.3
20	0.54363477	67.402592	13.40	3.78 ± 0.47	108.1 ± 3.5	4.60 ± 0.31	108.2 ± 1.9	4.21 ± 0.23	106.3 ± 1.5	3.76 ± 0.21	109.0 ± 1.6
23	0.55624163	67.436586	13.84	6.85 ± 0.75	101.9 ± 3.1	6.10 ± 0.42	109.7 ± 1.9	5.97 ± 0.27	112.9 ± 1.3	5.57 ± 0.23	110.9 ± 1.2
66	0.62357699	67.428952	12.95	6.81 ± 0.50	107.5 ± 2.1	7.14 ± 0.28	106.5 ± 1.1	6.99 ± 0.19	107.7 ± 0.8	6.34 ± 0.16	108.1 ± 0.7
69	0.47981658	67.394837	14.06	6.16 ± 0.74	111.3 ± 3.3	6.62 ± 0.47	104.4 ± 2.0	6.74 ± 0.35	107.5 ± 1.5	5.39 ± 0.33	103.3 ± 1.7
114	0.58320121	67.468772	12.43	5.37 ± 0.28	97.8 ± 1.5	5.50 ± 0.17	102.5 ± 0.9	5.39 ± 0.11	96.7 ± 0.6	4.66 ± 0.13	98.3 ± 0.8
130	0.55160126	67.476766	12.61	5.84 ± 0.34	99.0 ± 1.6	7.17 ± 0.19	105.1 ± 0.7	6.80 ± 0.11	98.4 ± 0.5	6.14 ± 0.11	98.2 ± 0.5
157	0.50636486	67.482452	14.51	6.89 ± 0.96	94.8 ± 3.9	7.06 ± 0.57	100.8 ± 2.3	6.62 ± 0.40	99.0 ± 1.7	5.74 ± 0.35	94.6 ± 1.7
169	0.60818307	67.484653	13.43	6.86 ± 0.48	95.0 ± 2.0	7.29 ± 0.28	102.6 ± 1.1	7.16 ± 0.17	99.2 ± 0.7	6.34 ± 0.19	100.5 ± 0.8
186	0.52564189	67.495438	13.72	5.44 ± 0.67	99.7 ± 3.5	5.95 ± 0.36	99.9 ± 1.7	5.70 ± 0.20	100.3 ± 1.0	5.00 ± 0.19	101.0 ± 1.1
234	0.58994890	67.508870	14.22	4.81 ± 0.65	96.4 ± 3.8	5.66 ± 0.39	106.6 ± 1.9	5.16 ± 0.26	101.3 ± 1.4	4.57 ± 0.31	99.0 ± 1.9
239	0.30857984	67.443113	12.94	2.46 ± 0.43	81.1 ± 4.8	1.98 ± 0.28	80.4 ± 3.5	2.24 ± 0.18	82.7 ± 2.2	1.78 ± 0.21	83.5 ± 3.2
247	0.44508728	67.507038	10.09	6.14 ± 0.12	106.7 ± 0.6	6.80 ± 0.07	109.1 ± 0.3	6.48 ± 0.05	110.4 ± 0.2	5.87 ± 0.05	112.0 ± 0.2
307	0.34187817	67.503367	13.97	4.73 ± 0.97	103.0 ± 5.8	5.55 ± 0.45	105.7 ± 2.3	5.43 ± 0.27	107.1 ± 1.4	5.05 ± 0.22	108.3 ± 1.2
310	0.46585155	67.529885	12.48	6.39 ± 0.34	101.4 ± 1.5	5.59 ± 0.20	100.8 ± 1.0	5.77 ± 0.12	101.9 ± 0.6	4.89 ± 0.12	102.8 ± 0.7
316	0.29854431	67.489695	12.47	3.14 ± 0.36	74.9 ± 3.2	2.67 ± 0.27	76.3 ± 2.5	2.92 ± 0.19	75.3 ± 1.8	2.17 ± 0.24	66.9 ± 3.0
324	0.61096275	67.535161	14.13	7.21 ± 0.65	111.1 ± 2.6	6.98 ± 0.38	113.4 ± 1.5	6.63 ± 0.24	109.7 ± 1.0	6.00 ± 0.27	110.1 ± 1.3
367	0.75596949	67.523695	14.88	3.74 ± 1.00	88.1 ± 7.5	4.64 ± 0.54	105.1 ± 3.3	5.95 ± 0.33	99.6 ± 1.6	5.89 ± 0.36	101.2 ± 1.7
368	0.21731676	67.464417	13.93	3.10 ± 0.67	73.8 ± 6.0	2.54 ± 0.43	64.8 ± 4.4	2.72 ± 0.29	76.7 ± 3.0	2.55 ± 0.33	75.7 ± 3.6
382	0.77096790	67.524242	14.09	5.53 ± 0.57	100.7 ± 2.9	5.80 ± 0.37	102.7 ± 1.8	5.88 ± 0.25	100.9 ± 1.2	5.23 ± 0.31	102.4 ± 1.6
391	0.53020318	67.559531	13.15	6.61 ± 0.41	106.4 ± 1.8	6.76 ± 0.24	108.8 ± 1.0	6.86 ± 0.15	104.1 ± 0.6	6.13 ± 0.17	103.6 ± 0.8
418	0.56191788	67.566861	13.94	7.03 ± 0.59	104.4 ± 2.4	8.03 ± 0.35	109.4 ± 1.2	7.58 ± 0.24	103.6 ± 0.9	6.75 ± 0.29	103.1 ± 1.2
441	0.64887476	67.565940	12.14	7.48 ± 0.25	98.7 ± 0.9	8.15 ± 0.15	103.2 ± 0.5	7.91 ± 0.10	99.1 ± 0.4	7.16 ± 0.12	98.5 ± 0.5
454	0.58273633	67.573569	11.07	6.81 ± 0.14	99.1 ± 0.6	6.71 ± 0.09	102.9 ± 0.4	6.67 ± 0.06	98.1 ± 0.3	5.78 ± 0.08	99.2 ± 0.4
461	0.61191189	67.574077	13.72	7.45 ± 0.52	96.6 ± 2.0	8.10 ± 0.32	104.7 ± 1.1	7.45 ± 0.21	100.6 ± 0.8	6.42 ± 0.25	101.4 ± 1.1
486	0.70776450	67.569370	13.51	5.86 ± 0.71	97.1 ± 3.4	6.13 ± 0.28	102.9 ± 1.3	5.78 ± 0.14	98.4 ± 0.7	4.99 ± 0.13	100.6 ± 0.7
936	0.76152588	67.638797	12.63	6.39 ± 0.36	96.2 ± 1.6	6.53 ± 0.18	96.0 ± 0.8	6.23 ± 0.12	95.8 ± 0.5	5.41 ± 0.13	94.6 ± 0.6
988	0.58255340	67.659929	13.13	5.82 ± 0.46	102.7 ± 2.2	5.93 ± 0.23	100.9 ± 1.1	5.48 ± 0.17	99.2 ± 0.9	4.62 ± 0.19	102.5 ± 1.2
1067	0.74265875	67.657519	13.43	3.94 ± 0.50	99.3 ± 3.5	4.76 ± 0.26	96.8 ± 1.5	4.36 ± 0.18	97.2 ± 1.1	3.79 ± 0.20	98.1 ± 1.4
1154	0.76472099	67.663676	13.54	1.94 ± 0.49	87.7 ± 6.9	2.20 ± 0.27	87.1 ± 3.4	2.02 ± 0.20	83.8 ± 2.7	1.53 ± 0.24	85.2 ± 4.2
1213	0.74994583	67.670815	13.36	6.57 ± 0.55	88.9 ± 2.4	6.97 ± 0.26	89.1 ± 1.1	6.53 ± 0.17	89.2 ± 0.7	5.40 ± 0.17	90.2 ± 0.9
1446	0.82639705	67.684169	14.26	2.32 ± 0.71	106.3 ± 8.4	2.11 ± 0.39	99.5 ± 5.0	1.90 ± 0.28	95.2 ± 4.0	1.76 ± 0.34	89.3 ± 5.1
1580	0.67072198	67.712589	12.93	2.01 ± 0.38	90.7 ± 5.2	2.55 ± 0.21	88.5 ± 2.2	2.34 ± 0.15	92.4 ± 1.8	2.17 ± 0.18	92.7 ± 2.2
1684	0.72806296	67.716366	13.27	6.45 ± 0.68	92.5 ± 3.0	5.84 ± 0.25	96.2 ± 1.2	5.52 ± 0.13	96.7 ± 0.7	4.57 ± 0.12	98.0 ± 0.7

[a]Star IDs and V magnitudes, barring 16A, have been taken from P08.

Table 3. Observed $V(RI)_C$ polarization and polarization angles for 32 stars towards Be 59.

Star ID[a] (1)	RA (°) (J2000) (2)	Dec. (°) (J2000) (3)	V (mag)[a] (4)	$P_V \pm \epsilon$ (per cent) (5)	$\theta_V \pm \epsilon$ (°) (6)	$P_{R_C} \pm \epsilon$ (per cent) (7)	$\theta_{R_C} \pm \epsilon$ (°) (8)	$P_{I_C} \pm \epsilon$ (per cent) (9)	$\theta_{I_C} \pm \epsilon$ (°) (10)
47	0.47588896	67.411372	14.63	3.90 ± 0.61	95.7 ± 4.3	3.84 ± 0.46	97.2 ± 3.3	4.04 ± 0.41	105.9 ± 2.9
59	0.50411914	67.446995	14.88	4.50 ± 0.68	89.6 ± 4.3	4.58 ± 0.51	98.4 ± 3.1	4.64 ± 0.45	97.2 ± 2.7
62	0.55995352	67.388082	13.48	4.27 ± 0.22	106.7 ± 1.5	4.86 ± 0.13	106.1 ± 0.7	4.02 ± 0.12	107.5 ± 0.9
64	0.62424757	67.411543	14.56	5.74 ± 0.38	104.3 ± 1.9	6.05 ± 0.20	102.7 ± 0.9	5.49 ± 0.18	104.4 ± 0.9
92	0.52499704	67.462054	15.46	6.03 ± 0.92	103.0 ± 4.3	5.15 ± 0.68	101.9 ± 3.7	4.51 ± 0.56	99.0 ± 3.5
105	0.65972184	67.402794	13.65	6.17 ± 0.24	103.3 ± 1.1	5.71 ± 0.13	103.5 ± 0.6	4.84 ± 0.11	104.7 ± 0.6
120	0.68030330	67.416096	14.48	2.99 ± 0.37	106.7 ± 3.4	4.39 ± 0.20	113.0 ± 1.3	3.46 ± 0.19	113.7 ± 1.5
133	0.40192644	67.441032	14.94	6.31 ± 0.72	105.1 ± 3.2	5.59 ± 0.52	106.2 ± 2.6	4.44 ± 0.44	106.3 ± 2.8
195	0.73841635	67.396758	14.22	8.00 ± 0.32	100.0 ± 1.1	7.84 ± 0.17	100.5 ± 0.6	6.61 ± 0.15	101.0 ± 0.6
196	0.52409579	67.340231	13.46	2.40 ± 0.22	78.1 ± 2.5	2.08 ± 0.12	69.5 ± 1.6	1.91 ± 0.12	72.7 ± 1.7
198	0.70341898	67.367529	13.47	1.88 ± 0.24	65.7 ± 3.5	2.18 ± 0.15	79.5 ± 1.9	1.76 ± 0.17	75.4 ± 2.5
202	0.58241709	67.499918	14.19	5.61 ± 0.50	94.4 ± 2.6	5.24 ± 0.28	95.7 ± 1.5	4.72 ± 0.17	96.4 ± 1.0
215	0.53576488	67.333432	13.99	3.42 ± 0.30	72.8 ± 2.5	2.47 ± 0.18	74.6 ± 2.0	1.98 ± 0.19	76.1 ± 2.6
240	0.71675681	67.484199	14.61	7.49 ± 0.47	99.4 ± 1.8	8.23 ± 0.29	95.8 ± 1.0	7.27 ± 0.31	94.4 ± 1.2
317	0.32552520	67.501884	12.76	5.54 ± 0.28	110.2 ± 1.5	5.28 ± 0.14	108.1 ± 0.8	4.82 ± 0.12	108.6 ± 0.7
433	0.50950597	67.569704	13.22	5.80 ± 0.26	113.3 ± 1.2	4.64 ± 0.16	106.5 ± 1.0	4.28 ± 0.18	105.7 ± 1.1
503	0.23764401	67.540179	13.55	5.37 ± 0.33	102.0 ± 1.7	5.27 ± 0.21	103.3 ± 1.1	4.93 ± 0.21	103.2 ± 1.2
594	0.94921847	67.514749	11.25	1.94 ± 0.08	85.0 ± 1.1	1.64 ± 0.06	83.5 ± 1.1	1.44 ± 0.06	84.0 ± 1.2
689	1.00593420	67.502698	14.40	8.73 ± 0.35	88.2 ± 1.1	7.69 ± 0.23	87.8 ± 0.8	6.61 ± 0.17	88.9 ± 0.8
742	0.71032883	67.614514	14.87	5.88 ± 0.53	93.3 ± 2.5	5.44 ± 0.33	95.3 ± 1.7	5.43 ± 0.33	97.4 ± 1.7
828	1.04825650	67.522676	12.66	8.30 ± 0.15	91.2 ± 0.5	8.30 ± 0.10	90.0 ± 0.3	7.44 ± 0.08	90.6 ± 0.3
1028	1.11032740	67.533648	13.57	5.88 ± 0.23	105.8 ± 1.1	5.99 ± 0.15	107.0 ± 0.7	5.11 ± 0.12	107.5 ± 0.6
1106	1.19379620	67.469519	14.35	7.66 ± 0.33	100.8 ± 1.2	8.07 ± 0.24	98.5 ± 0.8	5.47 ± 0.19	102.4 ± 1.0
1135	1.15739640	67.522225	14.91	8.72 ± 0.45	96.6 ± 1.5	7.07 ± 0.29	100.9 ± 1.1	6.26 ± 0.21	99.0 ± 1.0
1190	1.11587840	67.561287	13.20	2.70 ± 0.20	90.3 ± 2.0	2.72 ± 0.15	88.2 ± 1.5	2.32 ± 0.13	87.2 ± 1.6
1273	0.70653826	67.681432	15.07	5.66 ± 0.57	93.9 ± 2.8	5.61 ± 0.37	94.8 ± 1.8	5.03 ± 0.38	97.4 ± 2.1
1305	0.69299158	67.686948	14.74	5.45 ± 0.49	97.8 ± 2.5	4.66 ± 0.30	99.1 ± 1.8	4.10 ± 0.31	94.4 ± 2.1
1312	0.59132421	67.692850	14.08	6.29 ± 0.37	101.1 ± 1.6	5.78 ± 0.20	103.8 ± 1.0	5.14 ± 0.17	106.1 ± 1.0
1451	1.17321310	67.574163	14.12	5.26 ± 0.30	104.3 ± 1.6	4.82 ± 0.20	108.0 ± 1.1	4.30 ± 0.16	109.2 ± 1.0
1513	0.82238181	67.690576	12.71	2.32 ± 0.19	86.3 ± 2.2	2.00 ± 0.14	88.3 ± 1.9	1.97 ± 0.17	93.3 ± 2.4
1523	1.27017620	67.506336	13.86	2.28 ± 0.27	87.9 ± 3.2	2.45 ± 0.20	88.2 ± 2.2	2.18 ± 0.17	84.5 ± 2.2
1569	1.22657310	67.557681	13.60	3.17 ± 0.24	88.9 ± 2.0	3.19 ± 0.17	86.7 ± 1.5	2.67 ± 0.15	88.3 ± 1.6

[a]From P08.

$E(B-V)_{max} \sim 1.8$ mag. The cluster members (shown by the open circles) seem to have spectral types earlier than A0. The TCD manifests the presence of a foreground population shown by the filled circles. The foreground population reddened by $E(B-V) = 0.4$ mag are found to be located at ~470 pc (P08). The other field star (late-type) population are shown by the filled diamonds.

The polarimetric observations can be used as a tool to identify member stars in a Galactic open cluster, particularly, when the field stars have colours similar to those of cluster members (Martínez et al. 2004; Vergne et al. 2007; Feinstein et al. 2008; Orsatti et al. 2010; Vergne et al. 2010; E11). The individual Stokes parameters of the polarization vector of the V band, P_V, given by $Q_V = P_V \cos(2\theta_V)$ and $U_V = P_V \sin(2\theta_V)$, are estimated for all the observed stars towards Be 59 and presented on a U_V versus Q_V plot, known as the Stokes plane, in Fig. 5.

The measured degree of polarization of a star depends on the cumulative amount of aligned dust grains that lie along the line of sight, and hence the degree of polarization would be similar, lower or higher depending on whether it is a member, foreground or background to the cluster. Likewise, the position angles of the cluster members would be similar, but different for foreground or background field stars as light from them could have contributions from different or additional dust components. Hence, the cluster members are expected to show a grouping in the U_V–Q_V plane, while non-members are expected to show a scattered distribution. Therefore, the U_V–Q_V plot could be a useful tool to identify the members of a cluster. The stars with intrinsic polarization (due to asymmetric distribution of matter around young stellar objects) and/or rotation in their polarization angles may also create scattered distribution in the U_V–Q_V plane. A nebulous background in the case of star-forming regions would also create small intrinsic polarization and hence possibly the scattered distribution.

Fig. 5 shows two prominent groupings around $U_V \sim -2.5$ and $Q_V \sim -5.5$ (first group) and $U_V \sim 1.0$ and $Q_V \sim -2.0$ (second group). The grouping at $U_V \sim -2.5$ and $Q_V \sim -5.5$ should be due to the cluster members. 50 per cent (13 out of 27) of the field stars, identified on the basis of $(U-B)-(B-V)$ TCD (Fig. 4), are found mainly around $U_V \sim 1.0$ and $Q_V \sim -2.0$. The remainder of the probable field stars show a scattered distribution in the U_V–Q_V plot; however, some of the probable field stars are found to mingle with the probable cluster members. To further elucidate the membership, we plot a box with the dashed line in the U_V–Q_V plot having boundaries of mean $P_V \pm \sigma_{P_V}$ (6.22 ± 1.21 per cent) and mean $\theta_V \pm \sigma_{\theta_V}$ (102° ± 6°) obtained using the probable member stars (open circles) identified in Fig 4. The stars shown with the open circles and lying within the 1σ box of the mean P_V and θ_V could be probable members of the cluster. It is apparent from the $(U-B)$–$(B-V)$ TCD in Fig. 4 that the majority of the stars located

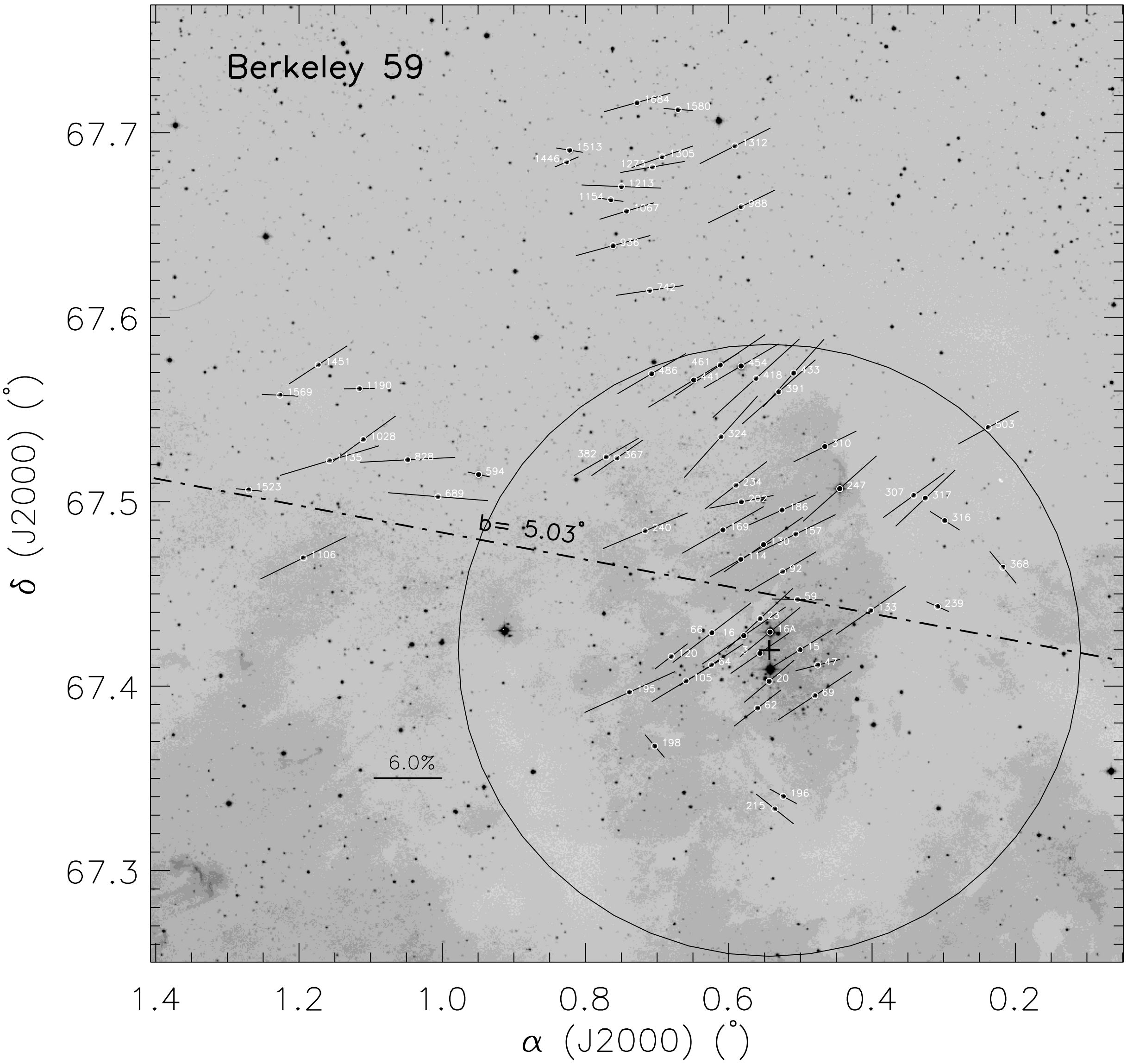

Figure 1. The stellar polarization vectors are superimposed on a 21 × 19 arcmin^2 *R*-band DSS II image of the field containing Be 59. The length of the polarization vector is proportional to P_V. A vector with a polarization of 6 per cent is drawn for reference. The dot–dashed line is the GP at $b = 5\overset{\circ}{.}03$. The plus symbols represent the cluster centre, RA = $00^{\rm h}02^{\rm m}10\overset{\rm s}{.}4$, Dec. = 67°25′10″. The cluster radius is shown with a big circle of ∼10 arcmin (P08). The stars observed are identified using the star identification numbers from P08. North is at the top and east is to the left.

within the 1σ box follow the general reddening of the cluster region, hence are probable members of the cluster.

Stars #59, 120, 689, 828 and 1213 are located significantly away from the 1σ box. Star #59 (P_V = 4.5 per cent, θ_V = 90°) and star #120 (P_V = 3.0 per cent, θ_V = 107°), even though located spatially within the cluster region (see Fig. 1) and with photometric colours consistent with membership, their P_V value or θ_V value is not comparable to the cluster region (see Fig. 5), so are considered as non-members. Stars #689, 828 and 1213 are located outside the cluster region. These stars show relatively large polarization (∼6.6 to 8.7 per cent), but their θ_V values (∼88° to 91°) are significantly different from those of probable cluster members (Tables 2 and 3) and are comparable to the GP. Hence, these are considered as non-members. Stars #23, 195, 247, 324, 391, 418, 441, 433 and 461 are distributed outside but near the boundary of the 1σ box. Barring stars #23, 195 and 324, these stars have a relatively higher value of $\overline{\epsilon}$ (cf. Fig. 10 shown later; Section 4), indicating rotation in their polarization angles. These stars have $E(B - V)$ in the range of 1.4–1.8 mag (cf. Fig. 4), so could be members of the cluster. Three stars, namely stars #20, 62 and 367, are also located near the boundary of the 1σ box. The P_V values of these stars are in the range of 4.3–4.6 per cent which is the lower limit of P_V value for the cluster member stars (see Tables 2 and 3). The θ_V values range from 105° to 108°. These could also be members of the cluster.

There seems to be a less prominent grouping around $U_V \sim -1.0$ and $Q_V \sim -5.0$ consisting of stars #202, 742, 936, 1067, 1273, 1305 and 1684 (cf. Fig. 5). We refer to this group as the third group. Interestingly, all these stars (except star #202) are located spatially at the same region towards the northern part of the cluster Be 59. This group of stars are located near the edge of the 1σ box. The mean value of P_V (5.68 ± 0.53 per cent) is comparable to the P_V values of the cluster region. However, the mean θ_V (=95° ± 2°) is significantly different from that in the cluster region. These stars are considered as field stars.

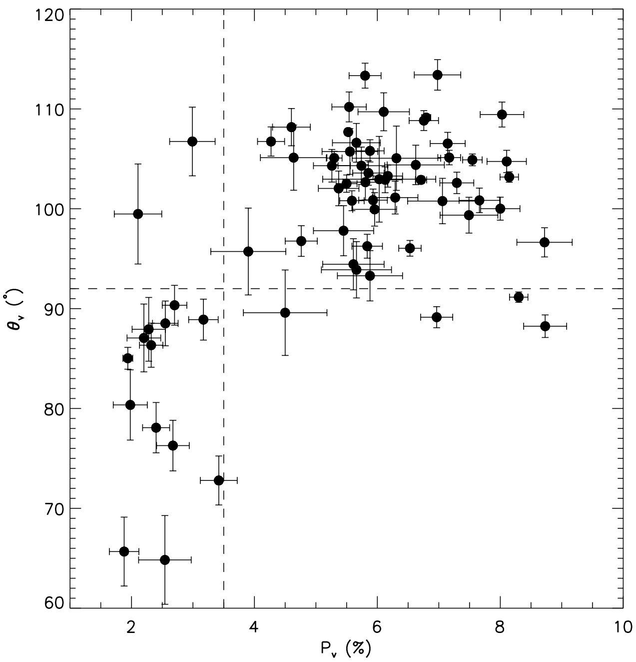

Figure 2. Polarization angle versus polarization in the *V* band for 69 stars towards Be 59. The dashed lines are drawn to show the two clearly separated groupings among the observed sample.

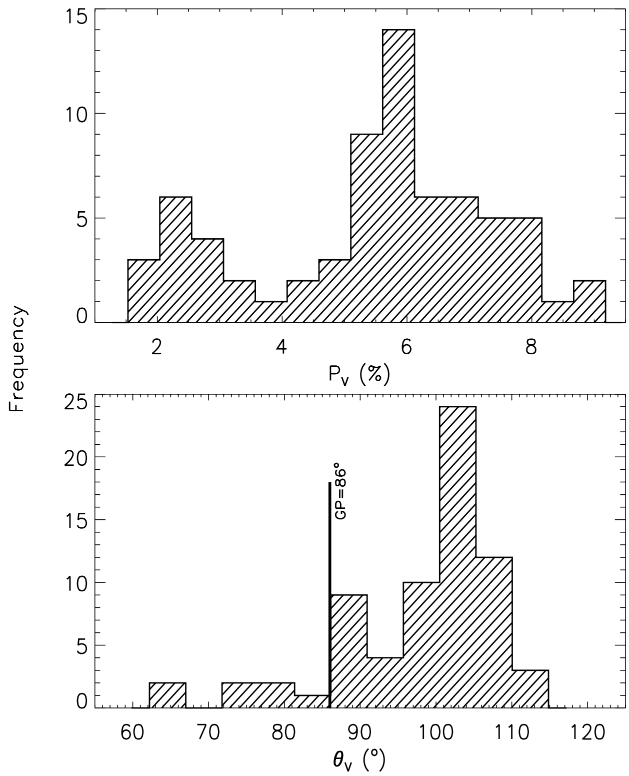

Figure 3. Histograms for P_V (upper panel) and θ_V (lower panel) for 69 stars towards Be 59. The thick line drawn in the lower panel represents the projection of the GP at 86°.

The colours of stars #1028, 1135 and 1451 are comparable to those of the cluster members and lie in the $E(B-V) \simeq 1.4$ to 1.8 mag range (presuming that these stars have spectral types earlier than A0). Star #1135 has P_V (8.12 ± 0.45 per cent) higher than those for cluster members; however, θ_V (96°.6 ± 1°.5) is smaller than the value for cluster stars. This star is located outside the 1σ box and also outside the estimated boundary of the cluster (Fig. 1); hence, this star is considered as a non-member. Stars #1028 and 1451 have P_V and θ_V values both comparable to those of the cluster members but located outside the boundary of the cluster; hence, the membership of these stars is uncertain.

Star #196 is located near the solar neighbourhood in the Q_V versus U_V diagram. Its colours are consistent with those of early-type members of the cluster, which yields $E(B-V) = 1.4$ mag, but its location in the Q_V–U_V diagram (Fig. 5) manifests that it should be a field star; hence, this star is considered as a field star for further discussion. Star #1106 is located near the 1σ box boundary (cf. Fig. 5). On the basis of its $(U-B)-(B-V)$ colours and its location outside the cluster boundary, we consider it as a non-member.

Stars #382, 503 and 988 are well separated from the cluster probable members in the $(U-B)$–$(B-V)$ TCD (cf. Fig. 4); however, they lie within the 1σ box in the Q_V–U_V plot (Fig. 5). Since stars #382 and 503 lie within the boundary of the cluster, and P_V and θ_V values are comparable to the cluster stars, these are considered as probable members. Star #988 lies outside the boundary of the cluster; hence, its membership is uncertain.

The probable members of the cluster identified using the U_V–Q_V and colour–colour diagrams are given in Table 4. The member, probable member and non-member stars are represented with 'M', 'PM' and 'NM', respectively. Stars with uncertainty in their membership determination are indicated with the '?' symbol.

Since cluster members seem to have spectral types earlier than A0 (see Fig. 4), the reddening $E(B-V)$ for the member stars has been estimated using the Q method (Johnson & Morgan 1953). As seen in Fig. 4, all the field stars have spectral types later than A0. The reddening $E(B-V)$ for field stars is estimated visually using the slide-fit method of ZAMS along the reddening vector. The estimated values of $E(B-V)$ are given in Table 4. The colours of stars #828 and 1213 suggest spectral types earlier than A0. The colours of star #689 suggest two reddening values, [$E(B-V) =$ 0.70 mag for a spectral type later than A0, or $E(B-V) = 1.44$ mag for a spectral type earlier than A0). Star #1135 has $P_V = 8.72$ per cent, which is comparable to the cluster members; however, its θ_V value (96°.6) is different from the cluster region. Its colours also suggest two values of $E(B-V)$ (1.17 mag for a spectral type later than A0, or 1.42 mag for a spectral type earlier than A0). Similarly, colours for stars #1028, 1106 and 1451 have two possible values of reddening. These are mentioned in Table 4.

The colours of the third group of stars (#742, 936, 1067, 1273, 1305 and 1684) suggest that their $E(B-V)$ values are in the range of ∼0.95–1.30 mag. The location of star #936 in the $(U-B)$–$(B-V)$ TCD suggests an O/B spectral type. The mean values of P_V and θ_V for these stars are 5.69 ± 0.58 per cent and 96° ± 2°, respectively. This group of stars may lie between the foreground stars (∼470 pc) and the cluster. Assuming a mean $E(B-V) =$ 1.20 mag, the $V_0/(V-I)_0$ colour–magnitude diagram indicates that these stars are distributed at a distance of ∼700 pc.

Fig. 6 shows the distribution of P_V (left-hand panels) and θ_V (right-hand panels) for the identified foreground stars (first group and third group of stars) and cluster members. The mean and standard deviation of P_V and θ_V of these three groups of stars are given in Table 5 and also shown in Fig. 6. The mean values of Q_V and U_V are also listed in Table 5. Fig. 6 shows that the mean degree of polarization, polarization angle as well as the deviation of the

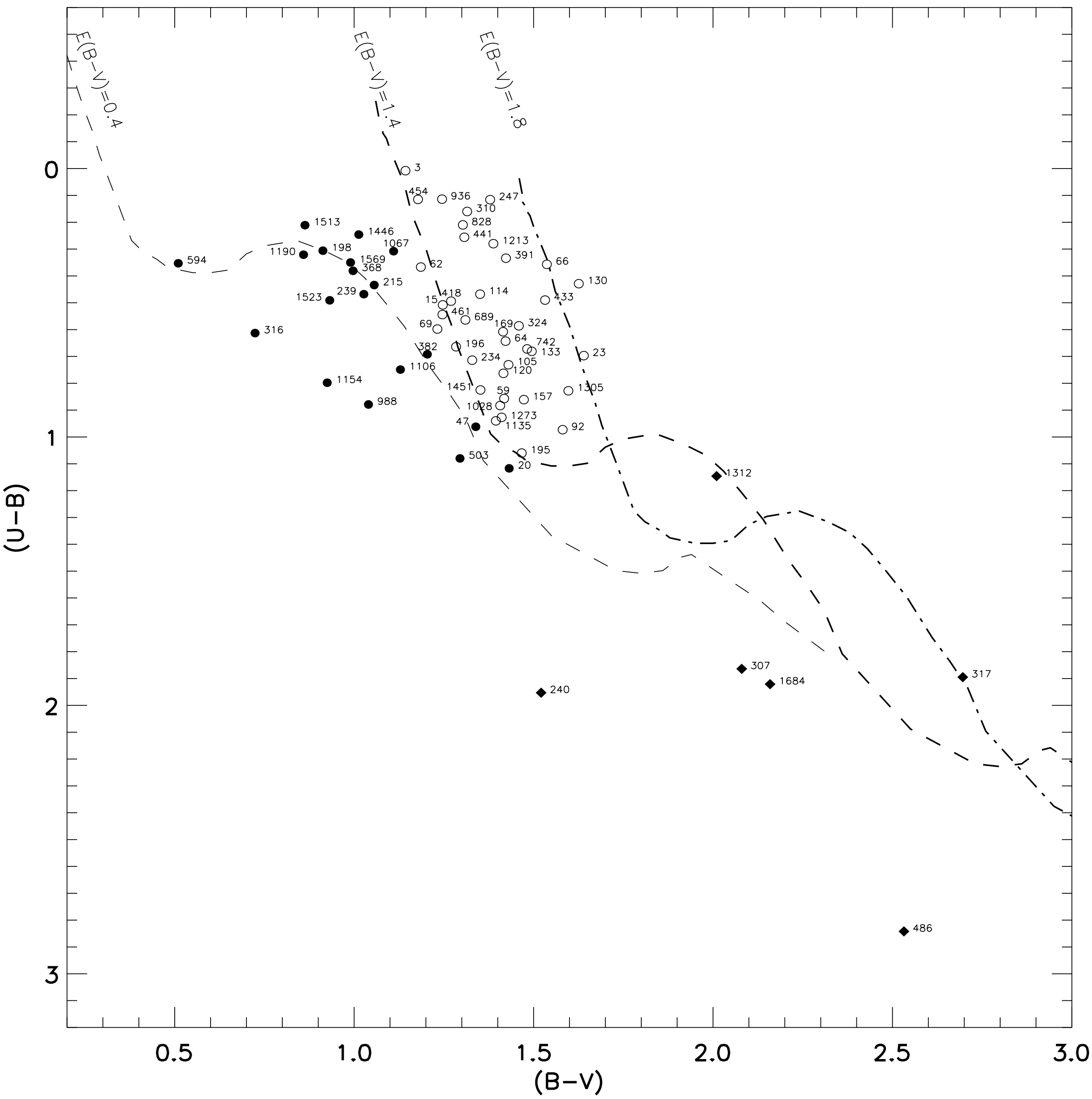

Figure 4. $(U - B)$ versus $(B - V)$ TCD. The theoretical ZAMS taken from Schmidt-Kaler (1982) is shifted along a reddening vector with an adopted slope of $E(U - B)/E(B - V) = 0.72$, to match the observed colours. The probable members and field stars are shown by the open and filled circles. The late-type stars are shown with the filled diamond symbols.

mean polarization angle from the GP increases systematically with increasing distance.

3.3 Dust distribution

The Stokes plane can be used effectively not only to determine the membership, but also to delineate the variations in the interstellar environments, for example, the distribution of dust layers, the role of dust layers in polarization, the associated magnetic field orientation, etc. The vector that connects two points in the Stokes plane represents the amount of polarization, while any change in the direction of vectors is related to a change in the polarization angle in our line of sight. If the dust grains are oriented/aligned uniformly (i.e. uniform magnetic field orientation), then the degree of polarization is expected to increase with distance, but the direction of polarization (polarization angle) should remain the same and hence the Stokes vector should not change its direction with increasing distance. For example, in the case of NGC 1893 (E11), the degree of polarization was found to increase with distance, whereas the direction of polarization remains almost constant (cf. their fig. 5).

To understand the dust distribution towards Be 59, we compare the polarization measurements of foreground stars, the stars of the third group, and the cluster members as shown in Fig. 7. The mean Stokes parameters of these three groups of stars are also marked with the large open circle, open square and filled circle, respectively, and are connected with the dashed line.

The individual polarization properties of the dust layers have been estimated by subtracting their foreground contribution, and the same are given in Table 6. The polarization measurements of the first group of foreground stars (mean $P_V = 2.44 \pm 0.45$ per

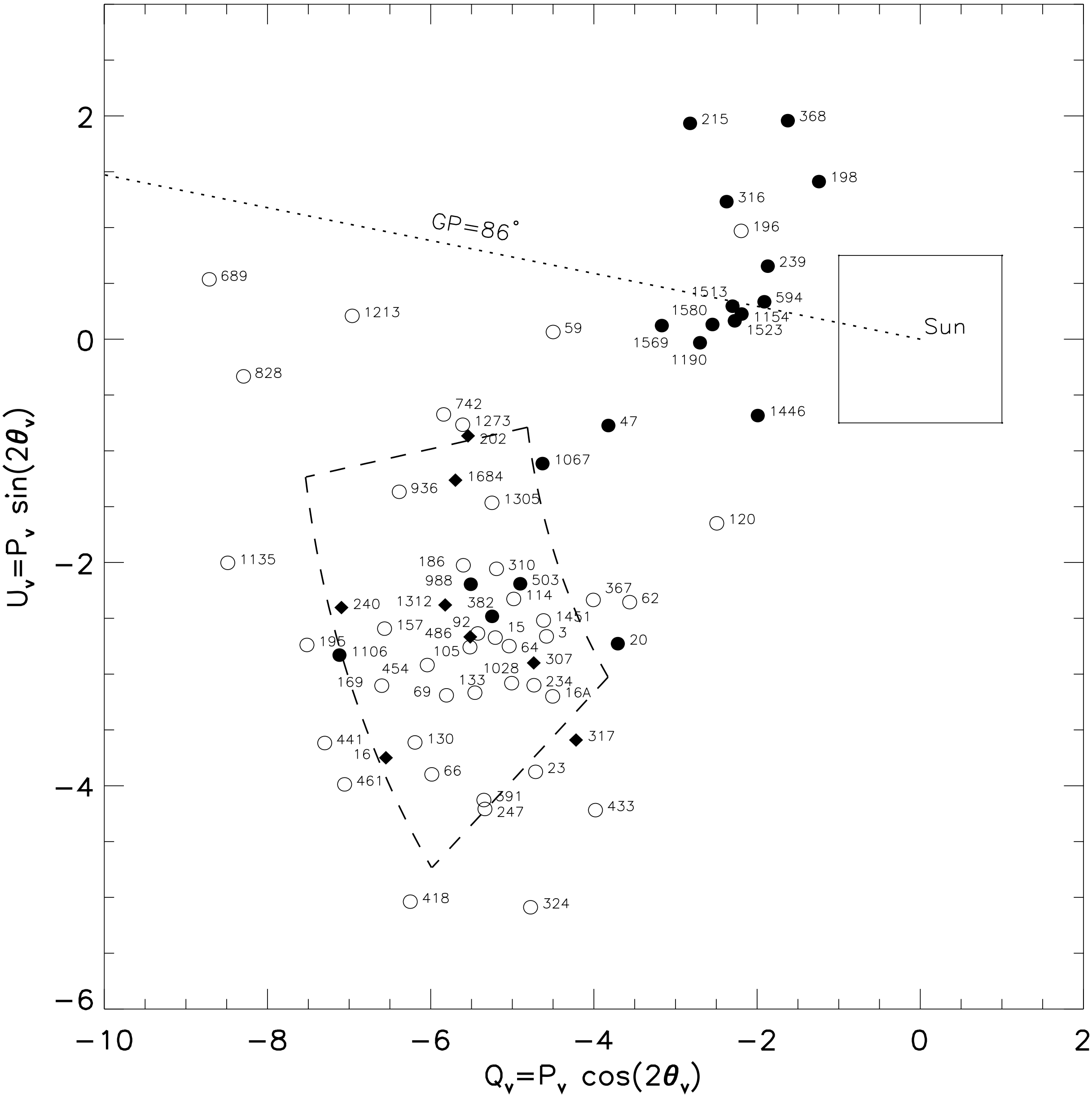

Figure 5. Q_V versus U_V of 69 stars. The symbols are the same as in Fig. 4. The GP is also drawn with the dotted line. The square covered by $Q_V = 0$ and $U_V = 0$ is the dustless solar neighbourhood. The 1σ box is drawn with the dashed line using the mean and standard deviation of $P_V \pm \sigma_{P_V} = 6.22 \pm 1.21$ per cent and $\theta_V \pm \sigma_{\theta_V} = 102° \pm 6°$, respectively.

cent and mean $\theta_V = 82° \pm 10°$) located at ∼470 pc indicate the presence of a dust layer at ≲470 pc. The orientation of magnetic field of this layer is found to be comparable to the GP. The third group of stars, lying between the first group and the cluster Be 59, show different polarization measurements ($P_V = 5.55 \pm 0.41$ per cent and $\theta_V = 95° \pm 2°$) from those of the first group or the cluster members. This fact manifests that there must be another dust layer at a distance ≳500 pc that polarizes the starlight of the second group of stars by ∼3.5 per cent (see Table 6). The dust grains in this dust layer are found to be aligned significantly differently (∼104°, see Table 6) from those in the first dust layer (∼82°). The polarization measurements for cluster members ($P_V = 6.34 \pm 1.05$ per cent and $\theta_V = 105° \pm 4°$) also indicate different polarization properties of intracluster dust. Table 6 suggests that the intracluster medium also polarizes the cluster members by ∼2.20 per cent. The dust grains of the intracluster medium are aligned significantly differently (∼135°) from those in the two foreground dust layers. The polarization angles found to increase with increase in distance from the Sun (cf. Table 6 and Fig. 7). This systematic change in the alignment of dust grains may cause *depolarization* (less polarization efficiency). This issue will be discussed in the ensuing section.

To further study the dust distribution for a distance ≲500 pc towards the direction of Be 59, we select stars with polarization measurements from the catalogue of Heiles (2000) and having *Hipparcos* parallax measurements (van Leeuwen, 2007) in a 10° radius around Be 59. We selected stars by applying the following criteria: (i) $P_V > 0.1$ per cent; (ii) ratio of parallax error to the parallax, that

Table 4. The $E(B-V)$ values estimated using the $(U-B)$–$(B-V)$ TCD. The membership information is also mentioned against each star ID.

Stars with $BV(RI)_C$ passband data			Stars with $V(RI)_C$ passband data		
Star ID[a]	$E(B-V)$ (mag)	Membership	Star ID[a]	$E(B-V)$ (mag)	Membership
(1)	(2)	(3)	(4)	(5)	(6)
3	1.41	M	47	0.43[b], 1.20	NM
15	1.38	M	59	0.63[b], 1.13[b]	NM
16	–	NM	62	1.35	M
16A	–	M	64	1.55	M
20	0.48[b], 1.40[b]	M	92	1.64	M
23	1.80	M	105	1.53	M
66	1.79	M	120	0.70[b], 1.06[b]	NM
69	1.33	M	133	1.63	M
114	1.52	M	195	1.47	M
130	1.87	M	196	0.57[b]	NM
157	1.54	M	198	0.40[b]	NM
169	1.55	M	202	–	NM
186	–	M	215	0.63[b]	NM
234	1.41	M	240	–	NM
239	0.33[b], 0.65[b]	NM	317	1.81[b]	NM
247	1.67	M	433	1.74	M
307	0.95[b]	NM	503	1.30	PM
310	1.58	M	594	0.35[b], 0.51	NM
316	0.65[b]	NM	689	0.70[b], 1.44	NM
324	1.61	M	742	0.95[b], 1.61	NM
367	–	M	828	1.54	NM
368	0.55[b]	NM	1028	1.14[b], 1.45	?
382	1.26	PM	1106	1.17	NM
391	1.65	M	1135	1.17[b], 1.42	NM
418	1.41	M	1190	0.46[b]	NM
441	1.53	M	1273	0.56[b], 1.16[b]	NM
454	1.42	M	1305	0.95[b], 1.17[b]	NM
461	1.36	M	1312	1.34[b]	NM
486	–	NM	1451	1.08[b], 1.40	?
936	1.50	?	1513	0.30[b]	NM
988	1.05[b]	?	1523	0.63[b]	NM
1067	0.55[b], 1.27	NM	1569	0.45[b]	NM
1154	0.85[b]	NM			
1213	1.63	NM			
1446	0.45[b]	NM			
1580	–	NM			
1684	0.95[b] NM				

Notes. M: members; NM: non-members; PM: probable members; ?: stars with uncertainty in their membership.
[a]From P08.
[b]$E(B-V)$ values were obtained using the slide-fit method.

is, $\sigma_{\pi_H}/\pi_H \lesssim 0.5$; and (iii) stars without having any emission features or photometric variability (with the help of SIMBAD). Fig. 8 shows polarization versus distance (upper panel) and polarization versus polarization angle (lower panel) for the stars studied in this work (same symbols as in Fig. 7) as well as the stars (shown with the dots) from Heiles (2000). Fig. 8 indicates a sudden increase in polarization at ∼300, ∼500 and ∼700 pc, which suggests the presence of three dust layers at ∼300, ∼500 and ∼700 pc towards Be 59.

As shown in the lower panel, the polarization angles of the Heiles stars (dots) are distributed randomly, which indicates that the magnetic field orientation in the nearby but an extended region towards the direction of Be 59 is not as organized as that in the cluster region. Hence, the magnetic field in the intracluster medium seems to be more confined.

Neckel & Klare (1980) have studied the reddening distribution in the GP with $|b| \lesssim 7^\circ\!.6$ using the extinction and distances computed for individual stars. The A_V map towards the direction of Be 59 by Neckel & Klare (1980) [see their fig. 6a, 4 (115/3)] shows an increase in A_V by ∼0.6 mag at a distance of ∼300 pc, indicating the presence of a dust layer at this distance. For a normal reddening law, $A_V \sim 0.6$ corresponds to $E(B-V) \simeq 0.20$ mag. This value of $E(B-V)$ yields a polarization of ∼1 per cent [$P = 5 \times E(B-V)$] which is in accordance with the dust layer at ∼300 pc as shown in Fig. 8. At ≃800 pc, A_V further increases and reaches ∼1 mag. A_V has a steep rise after 800 pc and at a distance of 1 kpc A_V is ∼3 mag corresponding to $E(B-V)$ of ∼1 mag, which is consistent with the cluster's foreground reddening. The present polarimetric results are therefore consistent with the reddening distribution given by Neckel & Klare (1980).

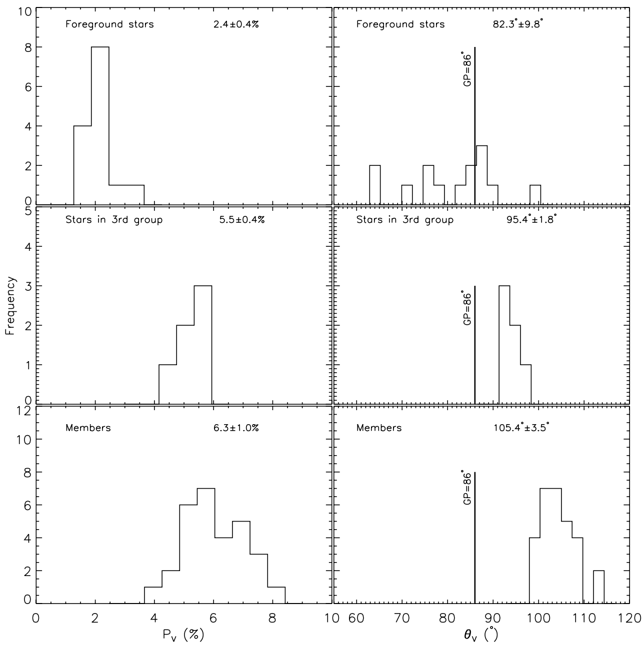

Figure 6. Histograms of P_V (left-hand panels) and θ_V (right-hand panels) for the foreground stars, stars in the third group and cluster members. For comparison, the GP is also drawn with the thick line at 86°. The mean and standard deviation values of P_V and θ_V for each group are also mentioned.

4 DUST PROPERTIES

The wavelength dependence of polarization towards many Galactic directions follows the empirical relation (Coyne, Gehrels & Serkowski 1974; Serkowski, Mathewson & Ford 1975; Wilking, Lebofsky & Rieke 1982)

$$P_\lambda = P_{\max} \exp[-K \ln^2(\lambda_{\max}/\lambda)], \quad (2)$$

where P_λ is the percentage polarization at wavelength λ and $P_{\max}$ is the peak polarization occurring at wavelength $\lambda_{\max}$. $\lambda_{\max}$ is a function of the optical properties and characteristic particle size distribution of aligned grains (Serkowski et al. 1975; McMillan 1978). The value of $P_{\max}$ is determined by the column density, the chemical composition, size, shape, and degree and orientation of the dust grains. The parameter K, an inverse measure of the width of the polarization curve, was treated as a constant by Serkowski et al. (1975), who adopted a value of 1.15 for all the stars. The Serkowski relation with $K = 1.15$ provides an adequate representation of the observations of interstellar polarization between wavelengths 0.36 and 1.0 μm. In one case, $P_{\max}$ and $\lambda_{\max}$ were obtained using the weighted non-linear least-squares fit to the measured polarization by adopting (1) $K = 1.15$ for stars having data in the $V(RI)_C$ passbands; or (2) $K = 1.66\lambda_{\max} + 0.01$ (Whittet et al. 1992) for stars having data in the $BV(RI)_C$ passbands. Table 7 lists $P_{\max}$, $\lambda_{\max}$, σ_1 and $\bar{\epsilon}$ for 69 stars. The estimated values of $P_{\max}$ and $\lambda_{\max}$ using $BV(RI)_C$ passband data are listed in the second and third columns, and those estimated using $V(RI)_C$ passband data are listed in the seventh and eighth columns, respectively. We also computed the parameters σ_1 (the unit weight error of the fit for each star),[2] which quantifies the departure of the data from the standard Serkowski law, and $\bar{\epsilon}$, the dispersion of the polarization angle for each star normalized by the average of the polarization angle errors (cf. Marraco, Vega & Vrba 1993). The estimated values of σ_1 and $\bar{\epsilon}$ using $BV(RI)_C$ passband data are listed in the fourth and fifth columns, whereas those estimated using $V(RI)_C$ passband data are in the ninth and tenth columns, of Table 7, respectively. Furthermore, $P_{\max}$ and $\lambda_{\max}$ for the 37 stars, which have data in the $BV(RI)_C$ passbands, have been calculated using the data of only three passbands, $V(RI)_C$, and $K = 1.15$. A comparison of the $P_{\max}$ and $\lambda_{\max}$ values obtained using the three- and four-passband data is shown in Fig. 9, which manifests a good agreement.

If the wavelength dependence of polarization is well represented by the Serkowski law, σ_1 should not be greater than 1.5 because of the weighting scheme. A higher value (>1.5) could be indicative of intrinsic stellar polarization (Waldhausen et al. 1999; Feinstein et al. 2008). The polarization angle rotation with wavelength ($\bar{\epsilon}$) also indicates the presence of an intrinsic polarization or a change in $\lambda_{\max}$ along the line of sight (Coyne 1974; Martin 1974). Systematic variations with wavelength in the position angle of the interstellar linear polarization of starlight may also be indicative of multiple dust layers with different magnetic field orientations along the line of sight (Messinger, Whittet & Roberge 1997). Following the above-stated criteria, we consider stars with $\sigma_1 > 1.5$ and $\bar{\epsilon} > 2.3$ as probable candidates to have intrinsic polarization and/or polarization angle rotation.

Fig. 10 plots the radial distance of stars from the centre of the cluster versus $\bar{\epsilon}$ (upper left-hand panel), $\bar{\epsilon}$ versus $P_{\max}$ (upper right-hand panel), the radial distance of stars versus σ_1 (lower left-hand panel), and σ_1 versus $\lambda_{\max}$ (lower right-hand panel). One can see that a significant number of stars show deviation from the normal distribution (14 stars have $\bar{\epsilon} > 2.3$, 19 stars have $\sigma_1 > 1.5$, and five stars have $\sigma_1 > 1.5$ as well as $\bar{\epsilon} > 2.3$, cf. Fig. 10 and Table 7). It is interesting to mention that the majority of foreground stars (12 out of 14) have $\bar{\epsilon} < 2.3$ and all the stars having $\bar{\epsilon} > 2.3$ are located within the cluster region, whereas the majority of the stars (10 stars) having $\sigma_1 > 1.5$ are located within the cluster region. About 40 per cent (28 out of 69) of the stars of the sample show the signatures of either intrinsic polarization or rotation in their polarization angles. 10 stars (#3, 16A, 133, 169, 195, 234, 367, 454, 689 and 1106) are found to be located in the near-infrared-excess zone (see Fig. 11). Six of them (#16A, 133, 195, 454, 689 and 1106) show intrinsic polarization, with $\sigma_1 > 1.5$. The upper right-hand panel of Fig. 10 indicates that a significant number of stars (12 stars) with $P_{\max} > 4.5$ per cent have $\bar{\epsilon} > 2.3$. The star #247 (BD +66° 1673) is located towards the north-western edge of the cluster. This star was previously classified with objective prism spectra as O9–B0 (Walker 1965; MacConnell 1968), but is re-classified later as O5 V((f))n (Majaess et al. 2008), making it the hottest star in the Cepheus OB4 association. The star's high temperature drives mass-loss via strong stellar winds (Yang & Fukui 1992; Gahm et al. 2006). Our polarimetric results indicate an intrinsic nature of polarization as it has $\sigma_1 = 1.83$ and $\bar{\epsilon} = 4.98$.

Another criterion to detect intrinsic stellar polarization is based on $\lambda_{\max}$. A star having $\lambda_{\max}$ much lower than the average value of the ISM (0.545 μm; Serkowski et al. 1975) is considered as a candidate to have an intrinsic component of polarization (Orsatti, Vega & Marraco 1998). In this study, only one star, star #215, has been found to have a much lower value of $\lambda_{\max} = 0.36 \pm 0.05$ μm. This star has $\sigma_1 = 5.5$.

4.1 Extinction law

To study the nature of the extinction law in the cluster region, we used the TCDs as described by Pandey, Ogura & Sekiguchi (2000)

[2] The values of σ_1 for each star are computed using the expression $\sigma_1^2 = \sum(r_\lambda/\epsilon_{p\lambda})^2/(m-2)$, where m is the number of colours and $r_\lambda = P_\lambda - P_{\max}\exp[-K\ln^2(\lambda_{\max}/\lambda)]$.

Table 5. The estimated mean values of P_V, θ_V, Q_V and U_V for the foreground stars, the stars in the third group and the cluster members. The distance information is also mentioned.

	$\overline{P_V}$ (per cent)	$\overline{\theta_V}$ (°)	$\overline{Q_V}$	$\overline{U_V}$	Number of stars	Distance (pc)
First group	2.44 ± 0.45	82 ± 10	$Q_{\rm f} = -2.35$	$U_{\rm f} = 0.65$	14	470
Third group	5.55 ± 0.41	95 ± 2	$Q_3 = -5.43$	$U_3 = -1.04$	6	700
Member stars	6.34 ± 1.05	105 ± 4	$Q_{\rm m} = -5.45$	$U_{\rm m} = -3.24$	29	1000

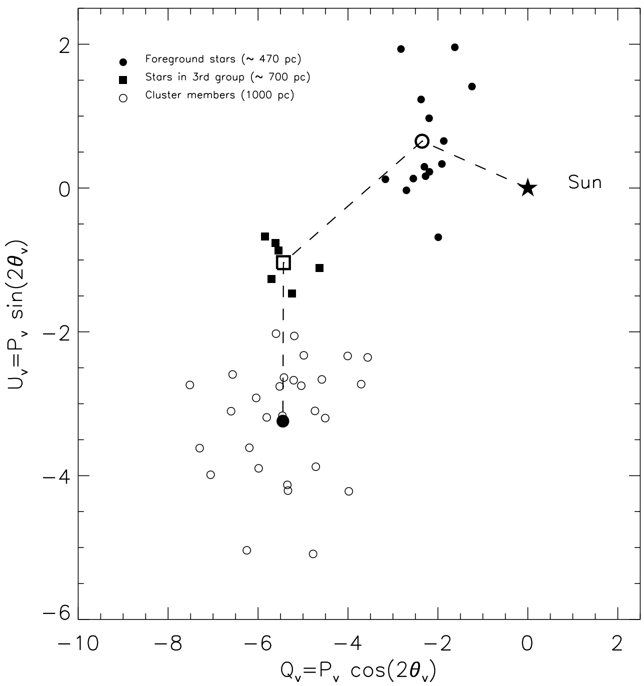

Figure 7. U_V versus Q_V diagram using the stars with known membership. The stars near the Sun, stars in the third group and cluster members are shown with the filled circles, filled squares and open circles, respectively. The mean Stokes parameters for these three groups of stars are also shown with the bigger open circle, open square and filled circle symbols, respectively. The filled star symbol denotes the position of the Sun at $Q_V = 0$ and $U_V = 0$.

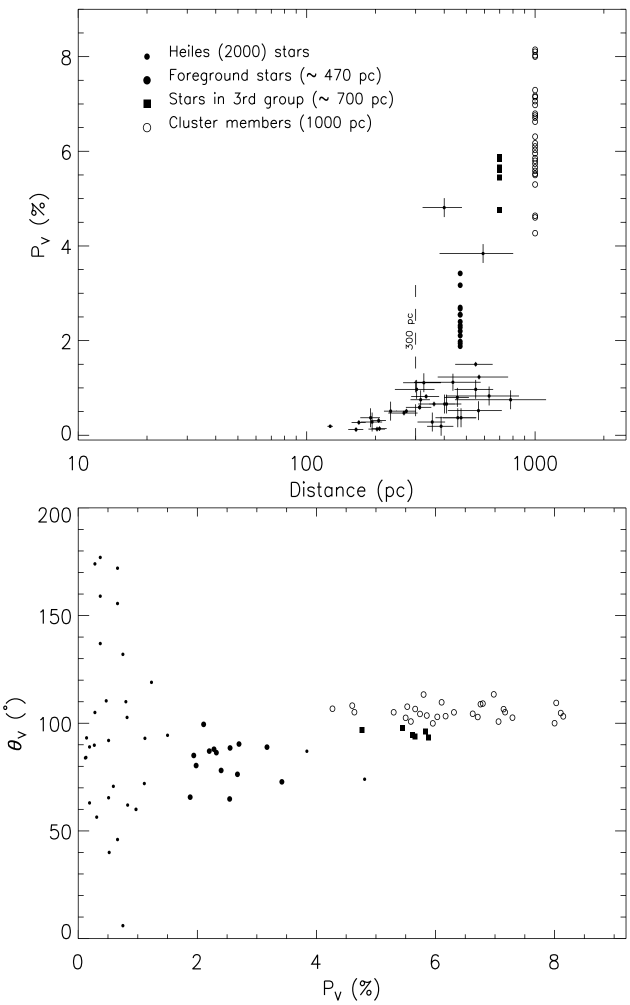

Figure 8. Distance versus polarization (upper panel) for the stars in the direction towards Be 59. Polarization and distance information for the stars located at distance $\lesssim$500 pc is obtained from Heiles (2000) and van Leeuwen (2007), respectively. Polarization versus polarization angle (lower panel).

and Pandey et al. (2003), in the form of $(V - \lambda)$ versus $(B - V)$, where λ is one of the wavelengths of the broad-band filters R, I, J, H, K or L, to separate the influence of the normal extinction produced by the diffuse ISM from that of the abnormal extinction arising within regions having a peculiar distribution of dust sizes (cf. Chini & Wargau 1990; Pandey et al. 2000). The $(V - \lambda)$ versus $(B - V)$ TCDs for the cluster region are shown in Fig. 12. The distribution of field stars follows a normal reddening law for the foreground ISM. The slopes of the distributions for cluster members, $m_{\rm cluster}$, are found to be 1.40 ± 0.08, 2.62 ± 0.15, 3.08 ± 0.20 and 3.31 ± 0.23 for the $(V - I)$, $(V - J)$, $(V - H)$ and $(V - K)$ versus $(B - V)$ TCDs, respectively. The ratios $\frac{E(V-\lambda)}{E(B-V)}$ and the ratio of total to selective extinction in the cluster region, $R_{\rm cluster}$, are derived using the procedure given by Pandey et al. (2003). Assuming the value of R_V for the diffuse foreground ISM to be 3.1, the ratios $\frac{E(V-\lambda)}{E(B-V)}$ yield $R_{\rm cluster} = 4.0 \pm 0.1$, which indicates an anomalous reddening law. P08 have also estimated an anomalous reddening law in the cluster

Table 6. The estimated net mean values of P_V, θ_V, Q_V and U_V due to the dust layers in front of the first and third groups of stars as well as due to the intracluster medium.

Dust layers	$\overline{P_V}$ (per cent)	$\overline{\theta_V}$ (°)	$\overline{Q_V}$	$\overline{U_V}$
In front of the first group of stars	2.44	82	$Q_{\rm f} = -2.35$	$U_{\rm f} = 0.65$
In front of the third group of stars	3.51	104	$Q_3 - Q_{\rm f} = -3.08$	$U_3 - U_{\rm f} = -1.69$
Intracluster medium	2.20	135	$Q_{\rm m} - Q_3 = -0.02$	$U_{\rm m} - U_3 = -2.20$

Table 7. P_{max}, λ_{max}, σ_1 and $\overline{\epsilon}$ for the observed 69 stars.

37 stars with $BV(RI)_C$ passband data					32 stars with $V(RI)_C$ passband data				
Star ID[a] (1)	$P_{max} \pm \epsilon$ (per cent) (2)	$\lambda_{max} \pm \epsilon$ (μm) (3)	σ_1 (4)	$\overline{\epsilon}$ (5)	Star ID[a] (6)	$P_{max} \pm \epsilon$ (per cent) (7)	$\lambda_{max} \pm \epsilon$ (μm) (8)	σ_1 (9)	$\overline{\epsilon}$ (10)
3	5.19 ± 0.08	0.55 ± 0.02	0.85	1.84	47	4.05 ± 0.28	0.69 ± 0.14	0.57	1.12
15	6.01 ± 0.12	0.62 ± 0.03	1.14	0.22	59	4.72 ± 0.31	0.68 ± 0.13	0.33	1.62
16	7.38 ± 0.09	0.57 ± 0.02	1.67	2.28	62	4.69 ± 0.14	0.58 ± 0.03	3.29	0.47
16A	5.57 ± 0.04	0.52 ± 0.01	3.54	3.08	64	6.02 ± 0.20	0.61 ± 0.04	0.79	0.45
20	4.36 ± 0.19	0.55 ± 0.06	0.85	0.33	92	6.00 ± 1.10	0.48 ± 0.10	0.83	0.43
23	6.36 ± 0.29	0.53 ± 0.06	0.87	1.63	105	6.25 ± 0.24	0.50 ± 0.02	3.44	0.67
66	7.18 ± 0.17	0.56 ± 0.03	0.15	0.79	120	3.91 ± 0.16	0.64 ± 0.07	3.49	2.13
69	6.67 ± 0.32	0.52 ± 0.06	1.12	1.30	133	6.59 ± 1.03	0.45 ± 0.07	1.68	0.27
114	5.56 ± 0.12	0.52 ± 0.03	0.94	3.99	195	8.23 ± 0.28	0.52 ± 0.02	2.91	0.61
130	6.94 ± 0.10	0.57 ± 0.02	1.82	5.87	196	2.31 ± 0.20	0.52 ± 0.06	1.06	2.37
157	7.08 ± 0.51	0.49 ± 0.08	0.23	1.45	198	2.08 ± 0.14	0.60 ± 0.09	1.42	3.00
169	7.32 ± 0.17	0.55 ± 0.03	0.56	2.86	202	5.54 ± 0.38	0.55 ± 0.05	0.95	0.64
186	5.91 ± 0.26	0.53 ± 0.05	0.52	0.22	215	3.98 ± 0.78	0.36 ± 0.05	5.50	0.72
234	5.41 ± 0.27	0.53 ± 0.07	0.69	2.57	240	8.03 ± 0.25	0.62 ± 0.05	1.38	2.13
239	2.26 ± 0.22	0.50 ± 0.12	1.03	0.46	317	5.50 ± 0.19	0.57 ± 0.03	0.97	1.22
247	6.69 ± 0.04	0.55 ± 0.01	1.83	4.98	433	5.66 ± 0.33	0.47 ± 0.03	3.40	4.28
307	5.52 ± 0.23	0.59 ± 0.06	0.29	0.63	503	5.40 ± 0.20	0.60 ± 0.05	0.36	0.59
310	6.02 ± 0.17	0.49 ± 0.03	2.13	1.00	594	1.95 ± 0.10	0.47 ± 0.03	2.81	0.75
316	2.99 ± 0.25	0.46 ± 0.09	1.31	1.10	689	8.73 ± 0.39	0.49 ± 0.02	3.57	0.41
324	7.10 ± 0.30	0.51 ± 0.05	0.35	1.48	742	5.74 ± 0.29	0.61 ± 0.07	0.94	1.05
367	6.01 ± 0.31	0.80 ± 0.06	0.51	1.88	828	8.44 ± 0.10	0.58 ± 0.01	2.49	1.48
368	2.81 ± 0.25	0.55 ± 0.13	0.64	1.86	1028	6.07 ± 0.18	0.55 ± 0.02	2.41	1.19
382	5.92 ± 0.20	0.57 ± 0.05	0.39	0.52	1106	8.58 ± 0.47	0.45 ± 0.02	7.15	1.29
391	6.93 ± 0.13	0.57 ± 0.03	0.74	2.99	1135	8.58 ± 0.55	0.47 ± 0.03	3.73	1.86
418	7.82 ± 0.22	0.55 ± 0.04	0.76	3.00	1190	2.77 ± 0.16	0.55 ± 0.05	1.02	1.05
441	8.10 ± 0.08	0.56 ± 0.02	0.75	5.89	1273	5.74 ± 0.39	0.57 ± 0.08	0.35	0.66
454	6.88 ± 0.06	0.53 ± 0.01	2.36	7.64	1305	5.39 ± 0.56	0.48 ± 0.06	1.38	0.73
461	7.95 ± 0.27	0.49 ± 0.04	0.87	3.16	1312	6.21 ± 0.31	0.53 ± 0.04	1.43	2.16
486	6.21 ± 0.29	0.48 ± 0.05	0.64	2.07	1451	5.21 ± 0.27	0.53 ± 0.04	1.35	2.25
936	6.58 ± 0.16	0.50 ± 0.03	0.72	0.52	1513	2.23 ± 0.17	0.54 ± 0.07	1.12	1.37
988	6.01 ± 0.28	0.46 ± 0.05	0.67	0.97	1523	2.40 ± 0.15	0.61 ± 0.09	0.54	0.49
1067	4.57 ± 0.20	0.52 ± 0.06	0.99	0.57	1569	3.26 ± 0.20	0.54 ± 0.05	1.22	0.54
1154	2.18 ± 0.35	0.44 ± 0.16	0.69	0.33					
1213	7.05 ± 0.31	0.46 ± 0.04	1.31	0.27					
1446	2.20 ± 0.50	0.44 ± 0.23	0.22	0.95					
1580	2.43 ± 0.12	0.57 ± 0.08	0.69	0.89					
1684	6.31 ± 0.44	0.41 ± 0.06	1.18	1.07					

[a]From P08.

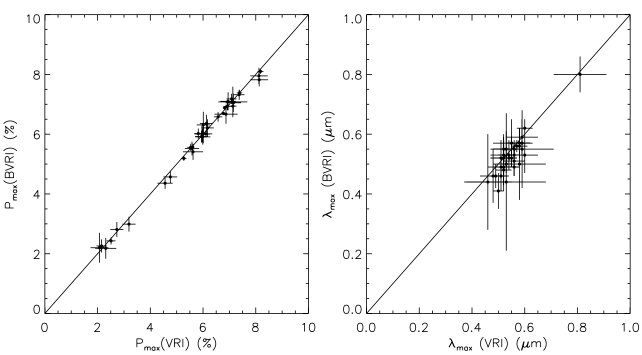

Figure 9. Left-hand panel: P_{max} computed using four passbands (using $K = 1.66\lambda_{max} + 0.01$) versus the same parameter but using three-passband data (using $K = 1.15$). Right-hand panel: the same as the left-hand panel, but for λ_{max}. Only 37 stars are used which have four-passband, $BV(RI)_C$, data (cf. Table 7).

region with $R_{cluster} = 3.7 \pm 0.3$, with a normal reddening law for the foreground diffuse ISM. In the central region of Be 59, MacConnell (1968) also found evidence for a large value (3.4–3.7) of R_V. Several studies have already pointed out an anomalous reddening law with a high R_V value in the vicinity of star-forming regions (see e.g. Pandey et al. 2003, and references therein); however, for the Galactic diffuse ISM, a normal value of $R_V = 3.1$ is well accepted. The higher than the normal values of R_V have been attributed to the presence of larger dust grains. There is evidence that within dark clouds accretion of ice mantles on grains and coagulation due to colliding grains change the size distribution towards larger particles. On the other hand, in star-forming regions, radiation from massive stars may evaporate ice mantles resulting in small particles. Here it is interesting to mention that Okada et al. (2003), on the basis of the [Si II] 35 μm-to-[N II] 122 μm ratio, suggested that efficient dust destruction is occurring in the ionized region of Be 59. Chini & Kruegel (1983) and Chini & Wargau (1990) have shown that either larger or smaller grains may increase the ratio of total to selective extinction.

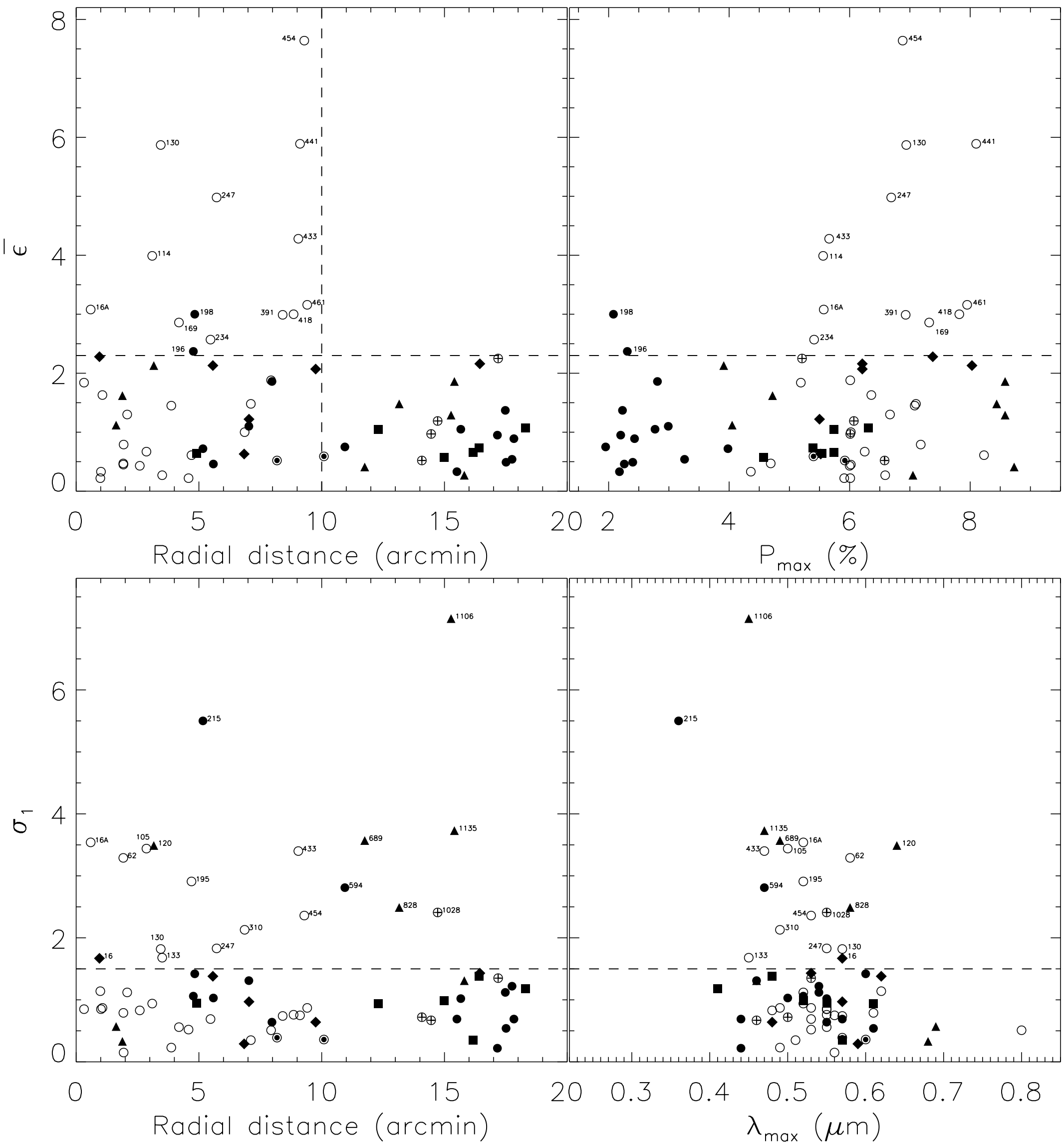

Figure 10. Upper panels: $\overline{\epsilon}$ versus radial distance of all stars from the centre of Be 59 and $\overline{\epsilon}$ versus $P_{\rm max}$. Lower panels: σ_1 versus radial distance of all stars from the centre of Be 59 and σ_1 versus $\lambda_{\rm max}$. The cluster members are shown with the open circles, foreground non-members with the filled circles, stars in the third group with the filled squares, late-type stars with the filled diamonds, other non-members with the filled triangles, probable members with the encircled filled circles, and stars with uncertainty in their membership with the encircled plus symbols.

The weighted mean value of $\lambda_{\rm max}$ for the cluster region was estimated to be 0.538 ± 0.004 µm. The mean value, within error, is comparable to the value measured in the general ISM (0.545 µm, Serkowski et al. 1975). Using the relation $R_V = (5.6 \pm 0.3)\lambda_{\rm max}$ (Whittet & Van Breda 1978), the value of R_V, the total to selective extinction, comes out to be 3.01 ± 0.16, which is in agreement with the average value ($R_V = 3.1$) for the Milky Way, but is in contradiction with the result obtained from the $(V - \lambda)$–$(B - V)$ TCDs. The mean value of $\lambda_{\rm max}$ for foreground stars is estimated at 0.498 ± 0.017 µm, which yields the R_V value as 2.79 ± 0.18 for the foreground diffuse ISM. This indicates a smaller value of R_V for the diffuse ISM towards the direction of the Be 59 ($l = 118\overset{\circ}{.}2$). There is much evidence in the literature that indicates significant variations in the properties of interstellar extinction along various Galactic directions. Whittet (1977) reported that the value of R_V in the GP can be represented by a sinusoidal function of the form $R_V = 3.08 + 0.17\sin(l + 175^\circ)$, which indicates a minimum value of R_V at $l \sim 95^\circ$. The above relation suggests a value of $R_V \sim 2.9$ towards the direction of Be 59 (i.e. $l = 118\overset{\circ}{.}2$). The study by Geminale & Popowski (2004) also suggests a lower value (∼2.9) towards Galactic longitude $l \sim 120^\circ$. Thus, the present estimation of $\lambda_{\rm max}$, and consequently the value of R_V for the diffuse ISM, is in agreement with the values reported in the literature. Hence, we conclude that R_V for the intracluster medium could be higher in comparison to that for the general diffuse matter towards the direction of Be 59. Here it is worthwhile to note that there is much evidence of variation of grain-size distribution towards the direction of Be 59.

4.2 POLARIZATION EFFICIENCY

The ratio of $P_{\rm max}/E(B - V)$ is known to be a measure of the polarization efficiency of the ISM and it depends mainly on the grain alignment efficiency, the magnetic field strength and the amount of

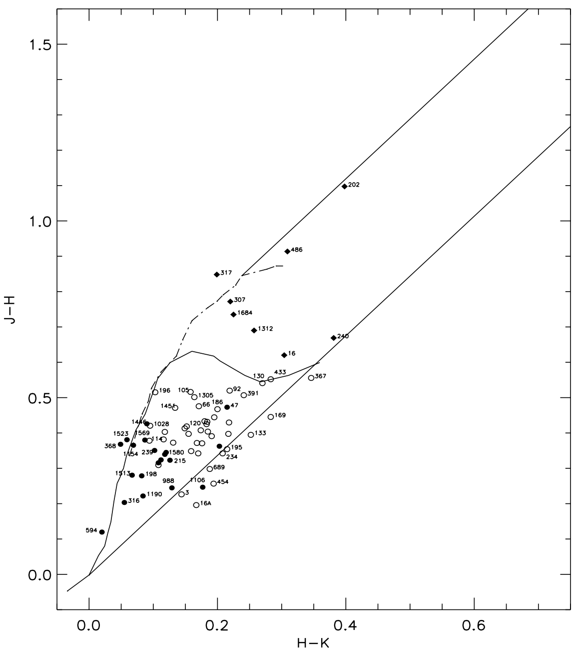

Figure 11. ($J - H$) versus ($H - K$) colour–colour diagram for all the observed stars in the direction towards Be 59. The data are taken from the 2MASS Point Source Catalog (Cutri et al. 2003). 2MASS data have been converted into the California Institute of Technology system using the relations provided by Carpenter (2001). The theoretical tracks for dwarfs and giants are drawn (Bessell & Brett 1988). Reddening vectors are also drawn (Cohen et al. 1981). The symbols are the same as in Fig. 4.

depolarization due to the radiation traversing clouds with different magnetic field directions. When the light passes through multiple dust layers, the resultant polarization may increase or decrease depending upon the orientation of the magnetic field in each dust layer (see e.g. Feinstein et al. 2003; Orsatti, Vega & Marraco 2003; Martínez et al. 2004; Vergne et al. 2007, 2010; E11). The observed polarization and extinction data towards a particular direction of the Galaxy provide important input to test the models dealing with the extinction and alignment of the grains. Fig. 13 displays the polarization efficiency diagram for the observed stars. The symbols are the same as in Fig. 10. It is well known that for the diffuse ISM the polarization efficiency cannot exceed the empirical upper limit given by, $P_{\max} = 3A_V \simeq 3R_V E(B - V) \simeq 9.3E(B - V)$ per cent (assuming $R_V = 3.1$, Hiltner & Johnson 1956; Serkowski et al. 1975) and the same is shown by a continuous line in Fig. 13. For the average ISM, Serkowski et al. (1975) have found that the polarization efficiency of the ISM follows the mean relation $P_{\max} \simeq 5E(B - V)$, which is shown by a dashed line. The recent estimate of the average polarization efficiency for the general diffuse ISM by Fosalba et al. (2002), which is valid for $E(B - V) < 1.0$ mag, is shown with a dot–dashed line.

Fig. 13 shows that the foreground stars (filled circles) are distributed along the dashed line, which suggests that the dust grains in the dust layer located at $\lesssim$470 pc have polarization efficiency comparable to the average polarization efficiency (~5 per cent per mag) of the diffuse ISM. The stars located at ~700 pc are shown with the filled squares. The colours of these stars indicate two values of $E(B - V)$ (see Table 4). We have used both values of $E(B - V)$ for these stars and those data are connected with the thin dot–dashed lines. In general, it seems that the dust layer located at $500 \lesssim d \lesssim 800$ pc also has an average polarization efficiency (i.e. 5 per cent per mag). The majority of the cluster members (open circles) are distributed below the dashed line, thereby indicating that the intracluster medium exhibits less polarization efficiency than the mean value for the diffuse ISM (~5 per cent per mag). The large dispersion in $P_{\max}$ (4–8 per cent) for cluster members is compatible with the differential reddening within the cluster (~1.4–1.7 mag).

The net polarization due to the intracluster medium is estimated to be ~2.2 per cent (cf. Table 6). The differential $E(B - V)$ due to the intracluster medium is ~0.3 mag. Thus, the net polarization efficiency due to the intracluster medium comes out to be ~7.3 per cent per mag, which is higher than that due to the diffuse ISM. The small dispersion in the mean value of θ_V (4°, Table 5) of cluster members also indicates a better alignment of dust grains in the intracluster medium. As discussed in Section 3.3, for the foreground stars of the first group and third group as well as the cluster members, the mean polarization angle changes with increasing distance systematically which may lead to the depolarization effect in the case of radiation from cluster members. Hence, the less polarization efficiency of the intracluster medium, as seen in Fig. 13, could be because of different alignments of dust grains in the foreground dust layers. A similar kind of depolarization effect has been observed towards Trumpler 27 by Feinstein et al. (2000), Hogg 22 and NGC 6204 by Martínez, Vergne & Feinstein (2004), and NGC 6124 by Vergne et al. (2010). Here it is interesting to mention that stars #418, 441 and 461, located at the northern periphery of the cluster, have the highest polarization efficiency among the cluster members. These stars have polarization efficiencies greater than the average value (5 per cent per mag) for the diffuse ISM. Four stars, #689, 828, 1106 and 1135, are located outside the boundary of the cluster and towards north-east of the cluster centre. These stars have the highest polarization ($P_V \sim 7.6$ to 8.7 per cent) and polarization efficiency greater than 5 per cent per mag. The $E(B - V)$ values of these stars range from ~1.20 to ~1.50 mag. Interestingly, all these four stars have their $\sigma_1 > 1.5$ (cf. Fig. 10), thereby indicating presence of intrinsic polarization.

5 SPATIAL VARIATION OF $E(B - V)$, P_V, θ_V AND $\lambda_{\max}$

Fig. 14(a) shows the spatial distribution of $E(B - V)$ as a function of radial distance from the centre of the cluster. The distribution reveals a lack of reddening material near the centre of the cluster. $E(B - V)$ increases away from the centre. The $E(B - V)$ value reaches its maximum at ~4 arcmin (~1.2 pc) and remains constant up to ~6 arcmin (1.8 pc). The $E(B - V)$ value decreases for radial distances > 6 arcmin. The spatial distribution suggests that the density of the reddening material is high at ~1.2–1.6 pc in comparison to that near the cluster centre. On the basis of one-dimensional raster-scan observations of the Sharpless 171 region (Be 59), Okada et al. (2003) have studied the spatial distribution of line intensities, representing the lowly ionized gas, highly ionized gas and photodissociation region (gas phases) as a function of radial distance from the cluster. The lines representing the neutral region (e.g. [O I] 63 μm, 146 μm; [C II] 158 μm; [Si II] 35 μm), lowly ionized region ([N II] 122 μm) and highly ionized region ([O III] 52 μm, 88 μm; [N III] 57 μm) show maxima at ~1 and ~4 pc, indicating the presence of high-density gas at these positions. Their fig. 6, showing 0.61-GHz continuum flux on the lines of the raster-scan observations, also indicated that the flux increases systematically with radial distance from the cluster centre and reaches the maximum at ~1.2 pc and remains constant up to ~1.7 pc. The flux shows a decreasing trend

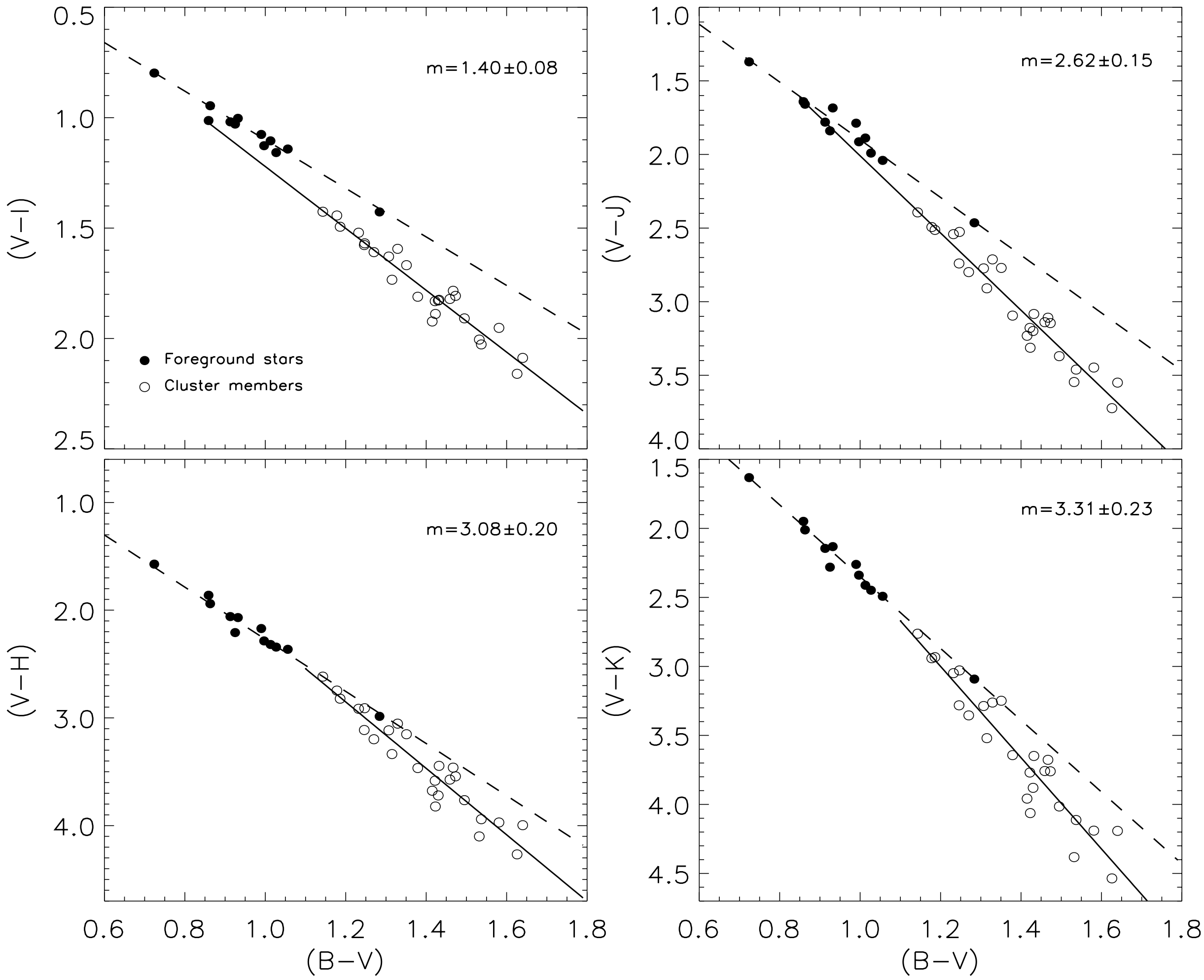

Figure 12. $(V-I)$, $(V-J)$, $(V-H)$, $(V-K)$ versus $(B-V)$ two-colour diagrams for the observed stars towards Be 59. The first group of foreground stars are shown with the filled circles, which follow the normal reddening by the general diffuse ISM (see table 3 of Pandey et al. 2003). The cluster members (open circles) show anomalous reddening as their slopes are significantly different from those of foreground stars. The fitted slopes for cluster members at each wavelength combination are overlaid on the figure.

for radial distance $\gtrsim$1.7 pc. The spatial distribution of the 0.61-GHz continuum flux agrees nicely with the $E(B-V)$ distribution shown in Fig. 14(a). Thus, it is clear that the density of the gas increases with the radial distance from the cluster centre with the maximum at ∼1 pc.

The spatial variation of P_V as a function of radial distance from the cluster centre (Fig. 14b) shows a systematic increasing trend with radial distance up to ∼5 arcmin; however, for radial distance $\gtrsim$5 arcmin, the distribution of P_V shows no trend but a significant scatter. The variation of P_V agrees well with the distribution of gas as discussed above, indicating that the average polarization efficiency in the core as well as in the corona of the cluster is the same. Fig. 14(c) shows the distribution of θ_V as a function of radial distance. The θ_V distribution also shows a systematic change with radial distance, in the same sense that the average θ_V value (∼110°) at the centre decreases to ∼100° at ∼5 arcmin. For radial distances $\gtrsim$5 arcmin, the distribution of θ_V shows a scattered distribution around 102°. On the basis of the θ_V distribution, we can conclude that the magnetic field orientation in the core of the cluster is significantly different from that in the coronal region, which is comparable to the magnetic field orientation of the third group of the stars (∼96°). We presume this could be either due to the molecular cloud at the centre being perturbed during the cloud collapse or due to strong stellar winds/supernova explosions.

Fig. 14(d) shows the spatial variation of λ_{max} obtained for identified members of the cluster, which manifests that λ_{max} is higher near the centre of the cluster. The average value of λ_{max} decreases up to ∼5 arcmin with increasing radial distance from the cluster centre. The distribution of λ_{max} suggests that the dust-grain size near the centre of the cluster is relatively higher in comparison to that in the coronal region. Okada et al. (2003), on the basis of the [Si II] 35 μm-to-[N II] 122 μm ratio, suggested that the efficient dust destruction is occurring in the ionized region. It is possible that the smaller dust grains might have been evacuated from the central region of the cluster due to strong stellar winds leaving relatively large dust grains in the central region of the cluster.

6 CONCLUSIONS

In this study, we have carried out polarimetric observations towards the direction of the young open cluster Be 59 in the $BV(RI)_C$ passbands. The aim of this study was to investigate the properties of dust grains in the ISM towards the direction of Be 59 as well as the properties of intracluster dust.

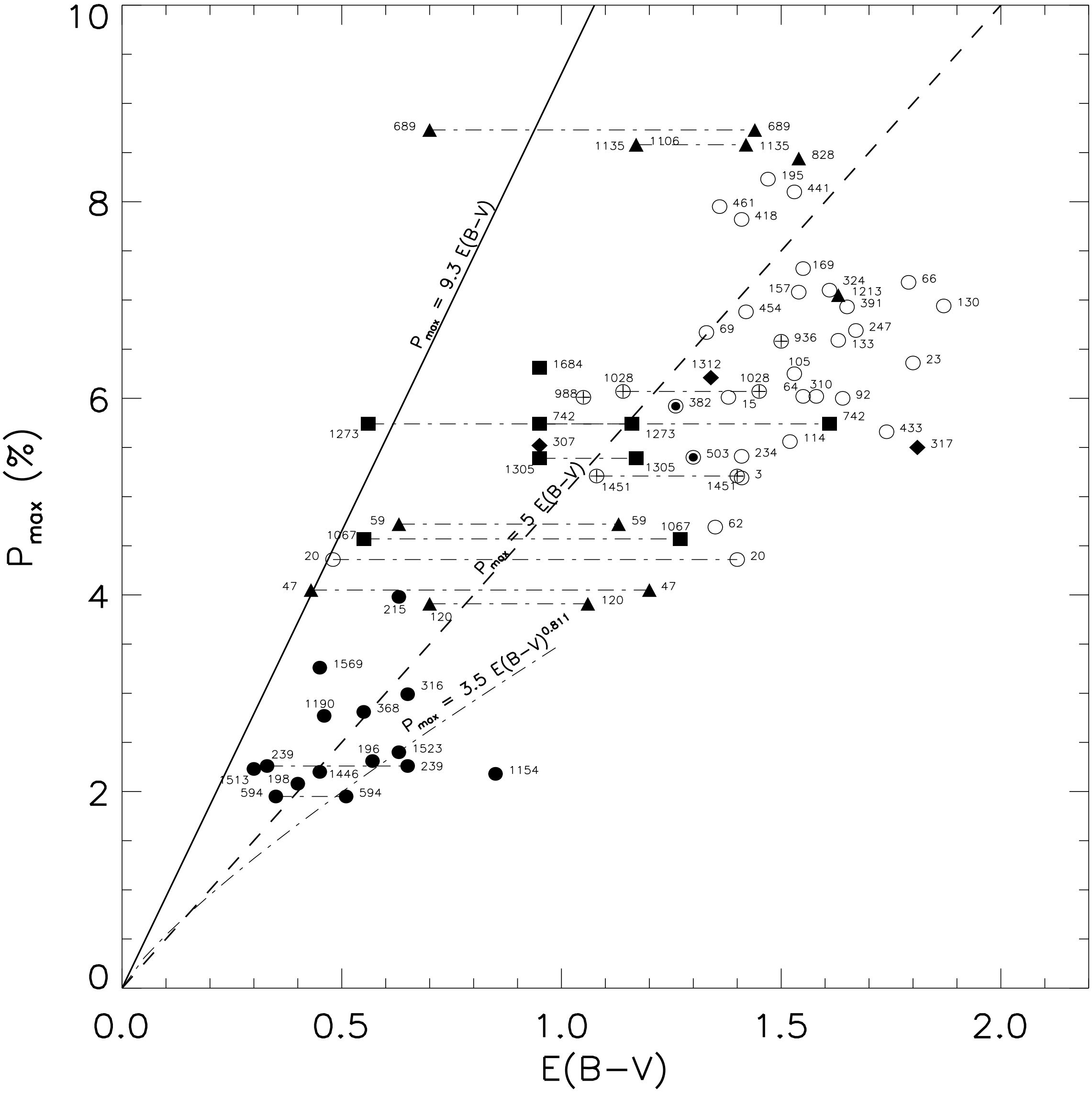

Figure 13. P_{max} versus $E(B-V)$ for the stars with available reddening (cf. Table 7). The symbols are the same as that of Fig. 10. The stars with two possible reddening values are connected by the thin dot–dashed line. The solid line represents the empirical upper limit relation for the polarization efficiency (by assuming $R_V = 3.1$) of $P_{max} = 9.3 \times E(B-V)$ (Serkowski et al. 1975). The dashed line represents the relation $P_{max} = 5 \times E(B-V)$ (Serkowski et al. 1975) and the dot–dashed line represents the relation $P_{max} = 3.5 \times E(B-V)^{0.8}$ by Fosalba et al. (2002).

The following are the main conclusions of this study:

(i) The distribution of P_V and θ_V suggests three dust layers towards the direction of Be 59 at ∼300, ∼500 and ∼700 pc. The total polarization due to these dust layers is found to be ∼0.2–1.0, ∼1.0–3.0 and ∼5.5 per cent. The magnetic field orientation of these dust layers is different from each other. The magnetic field orientation of the first dust layer (∼82°) is rather similar to that of the GP (86°).

(ii) We have further shown that the polarization measurements in combination with the $(U-B)$–$(B-V)$ colour–colour diagram provide a better estimation of the cluster members. The polarization measurements of the identified cluster members reveal that the net polarization due to the intracluster medium is estimated to be ∼2.2 per cent. About 40 per cent of the cluster members show the signatures of either intrinsic polarization or rotation in their polarization angles.

(iii) The TCDs of the identified cluster members reveal an anomalous reddening law in the cluster region. The weighted mean values of λ_{max} for the cluster region and for the foreground stars are estimated as 0.54 ± 0.01 and 0.50 ± 0.02 μm. The above estimate of λ_{max} for the foreground ISM indicates relatively smaller dust-grain sizes, consequently a smaller value of total-to-selective absorption ratio, $R_V = 2.79 \pm 0.18$, in comparison to the normal value for the diffuse ISM ($R_V = 3.1$). Thus, the mean λ_{max} value for the cluster region (0.54 ± 0.01 μm) suggests a relatively larger grain size in the cluster region in comparison to those in the general diffuse ISM towards the cluster region.

(iv) The foreground dust layers have polarization efficiency comparable to the average polarization efficiency (∼5 per cent per mag) of the diffuse ISM, whereas the majority of the cluster members indicate a smaller polarization efficiency for the intracluster medium. It indicates that the starlight of the cluster members might have been depolarized because of the non-uniform alignment of

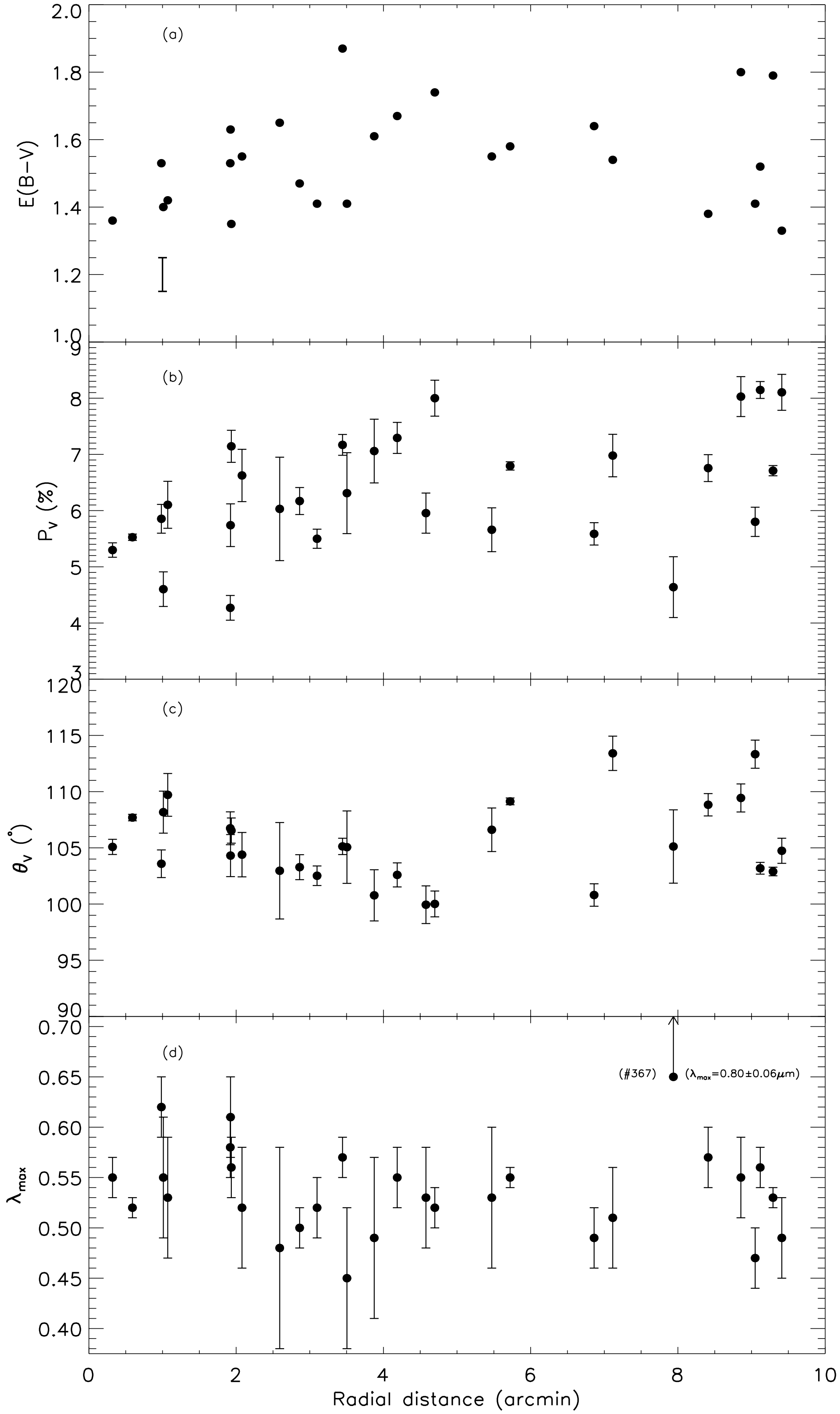

Figure 14. Radial variation of $E(B-V)$, P_V, θ_V and $\lambda_{\rm max}$ for only the cluster members. In the top panel, only the cluster members with $E(B-V)$ are used. The estimated error (0.05 mag) in $E(B-V)$ is also plotted for reference.

dust grains in the foreground dust layers and in the intracluster medium.

(v) The spatial distribution of $E(B - V)$ in the cluster region shows an increasing trend with radial distance. The polarization is also found to be systematically increasing with radial distance from the cluster centre. Both $E(B - V)$ and P_V values reach a maximum value at ∼4–5 arcmin (∼1.2–1.5 pc). θ_V as well as λ_{max} for the cluster members are found to decrease systematically with increasing radial distance.

ACKNOWLEDGMENTS

The authors are thankful to the referee, Prof. Michael S. Bessell, for his critical reading of the manuscript and several useful suggestions, which greatly improved the scientific content of this paper. This publication makes use of data from the 2MASS [a joint project of the University of Massachusetts and the Infrared Processing and Analysis Center /California Institute of Technology, funded by the National Aeronautics and Space Administration (NASA) and the National Science Foundation]. This research has made use of the WEBDA data base, operated at the Institute for Astronomy of the University of Vienna, as well as used the images from the Digitized Sky Survey, which was produced at the Space Telescope Science Institute under the US Government grant NAG W-2166. We have also used NASA's Astrophysics Data System and IRAF, distributed by National Optical Astronomy Observatories, USA. This research has made use of the SIMBAD data base, operated at CDS, Strasbourg, France. This work is partially supported by the Indo-Taiwan S&T programme.

REFERENCES

Aannestad P. A., Purcell E. M., 1973, ARA&A, 11, 309
Andersson B.-G., Pintado O., Potter S. B., Straižys V., Charcos-Llorens M., 2011, A&A, 534, 19
Bessell M. S., Brett J. M., 1988, PASP, 100, 1134
Carpenter J. M., 2001, AJ, 121, 2851
Chini R., Kruegel E., 1983, A&A, 117, 289
Chini R., Wargau W. F., 1990, A&A, 227, 213
Cohen J. G., Persson S. E., Elias J. H., Frogel J. A., 1981, ApJ, 249, 481
Coyne G. V., 1974, AJ, 79, 565
Coyne G. V., Gehrels T., Serkowski K., 1974, AJ, 79, 581
Cutri R. M. et al., 2003, The IRSA 2MASS All-Sky Point Source Catalog, NASA/IPAC Infrared Science Archive (http://irsa.ipac.caltech.edu/applications/Gator/)
Davis L., Jr, Greenstein J. L., 1951, ApJ, 114, 206
Eswaraiah C., Pandey A. K., Maheswar G., Medhi B. J., Pandey J. C., Ojha D. K., Chen W. P., 2011, MNRAS, 411, 1418 (E11)
Feinstein C., Baume G., Vázquez R., Niemela V., Cerruti M. A., 2000, AJ, 120, 1906
Feinstein C., Baume G., Vergne M. M., Vázquez R., 2003, A&A, 409, 933
Feinstein C., Vergne M. M., Martínez R., Orsatti A. M., 2008, 391, 447
Fosalba P., Lazarian A., Prunet S., Tauber J. A., 2002, ApJ, 564, 762
Gahm G. F., Carlqvist P., Johansson L. E. B., Nikolić S., 2006, A&A, 454, 201
Geminale A., Popowski P., 2004, Acta Astron., 54, 375
Heiles C., 2000, AJ, 119, 923
Hiltner W. A., Johnson H. L., 1956, ApJ, 124, 367
Johnson H. L., Morgan W. W., 1953, ApJ, 117, 313
Lazarian A., 2007, J. Quant. Spectrosc. Radiat. Transfer, 106, 225
Lazarian A., Hoang T., 2007, MNRAS, 378, 910
MacConnell D. J., 1968, ApJS, 16, 75
McMillan R. S., 1978, ApJ, 225, 880
Majaess D. J., Turner D. G., Lane D. J., Moncrieff K. E., 2008, J. Am. Assoc. Var. Star Obs., 36, 90
Marraco H. G., Vega E. I., Vrba F. J., 1993, AJ, 105, 258
Martin P. G., 1974, ApJ, 187, 461
Martínez R., Vergne M. M., Feinstein C., 2004, A&A, 419, 965
Messinger D. W., Whittet D. C. B., Roberge W. G., 1997, ApJ, 487, 314
Neckel Th., Klare G., 1980, A&AS, 42, 251
Okada Y., Onaka T., Shibai H., Doi Y., 2003, A&A, 412, 199
Orsatti A. M., Vega E., Marraco H. G., 1998, AJ, 116, 266
Orsatti A. M., Vega E. I., Marraco H. G., 2003, A&A, 408, 135
Orsatti A. M., Feinstein C., Vergne M. M., Martínez R. E., Vega E. I., 2010, A&A, 513, 75
Pandey A. K., Ogura K., Sekiguchi K., 2000, PASJ, 52, 847
Pandey A. K., Upadhyay K., Nakada Y., Ogura K., 2003, A&A, 397, 191
Pandey A. K., Sharma S., Ogura K., Ojha D. K., Chen W. P., Bhatt B. C., Ghosh S. K., 2008, MNRAS, 383, 1241 (P08)
Rautela B. S., Joshi G. C., Pandey J. C., 2004, Bull. Astron. Soc. India, 32, 159
Schmidt G. D., Elston R., Lupie O. L., 1992, AJ, 104, 1563 (S92)
Schmidt-Kaler Th., 1982, in Schaifers K., Voigt H. H., Landolt H., eds, Landolt-Bornstein, Vol. 2b. Springer-Verlag, Berlin, p. 19
Schulz A., Lenzen R., Schmidt T., Proetel K., 1981, A&A, 95, 94
Serkowski K., Mathewson D. S., Ford V. L., 1975, ApJ, 196, 261
van Leeuwen F., 2007, A&A, 474, 653
Vergne M. M., Feinstein C., Martínez R., 2007, A&A, 462, 621
Vergne M. M., Feinstein C., Martínez R., Orsatti A. M., Alvarez M. P., 2010, MNRAS, 403, 2041
Waldhausen S., Martínez R. E., Feinstein C., 1999, AJ, 117, 2882
Walker G. A. H., 1965, ApJ, 141, 660
Whittet D. C. B., 1977, MNRAS, 180, 29
Whittet D. C. B., van Breda I. G., 1978, A&A, 66, 57
Whittet D. C. B., Martin P. G., Hough J. H., Rouse M. F., Bailey J. A., Axon D. J., 1992, ApJ, 386, 562
Wilking B. A., Lebofsky M. J., Rieke G. H., 1982, AJ, 87, 695
Yang J., Fukui Y., 1992, ApJ, 386, 618

This paper has been typeset from a TEX/LATEX file prepared by the author.